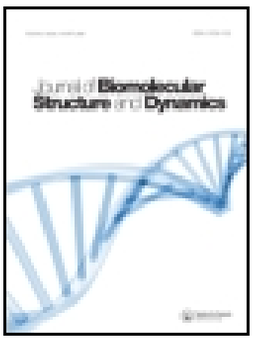

Taylor & Francis
Taylor & Francis Group

Journal of Biomolecular Structure and Dynamics

ISSN: (Print) (Online) Journal homepage: https://www.tandfonline.com/loi/tbsd20

Quantitative structure activity relationship studies of novel hydrazone derivatives as α-amylase inhibitors with index of ideality of correlation

Meenakshi Duhan , Jayant Sindhu , Parvin Kumar , Meena Devi , Rahul Singh , Ramesh Kumar , Sohan Lal , Ashwani Kumar , Sudhir Kumar & Khalid Hussain

To cite this article: Meenakshi Duhan , Jayant Sindhu , Parvin Kumar , Meena Devi , Rahul Singh , Ramesh Kumar , Sohan Lal , Ashwani Kumar , Sudhir Kumar & Khalid Hussain (2020): Quantitative structure activity relationship studies of novel hydrazone derivatives as α-amylase inhibitors with index of ideality of correlation, Journal of Biomolecular Structure and Dynamics, DOI: 10.1080/07391102.2020.1863861

To link to this article: https://doi.org/10.1080/07391102.2020.1863861

JOURNAL OF BIOMOLECULAR STRUCTURE AND DYNAMICS
https://doi.org/10.1080/07391102.2020.1863861

Quantitative structure activity relationship studies of novel hydrazone derivatives as α-amylase inhibitors with index of ideality of correlation

Meenakshi Duhan[a], Jayant Sindhu[b], Parvin Kumar[a], Meena Devi[a], Rahul Singh[a], Ramesh Kumar[a], Sohan Lal[a], Ashwani Kumar[c], Sudhir Kumar[d] and Khalid Hussain[e]

[a]Department of Chemistry, Kurukshetra University, Kurukshetra, India; [b]Department of Chemistry, COBS&H, CCS Haryana Agricultural University, Hisar, India; [c]Department of Pharmaceutical Sciences, Guru Jambeshwar University of Science and Technology, Hisar, India; [d]Department of MBB&B, COBS&H, CCS Haryana Agricultural University, Hisar, India; [e]Department of Applied Sciences and Humanities, Mewat Engineering College, Nuh, India

Communicated by Ramaswamy H. Sarma

ABSTRACT

The present manuscript describes the synthesis, α-amylase inhibition, *in silico* studies and in-depth quantitative structure–activity relationship (QSAR) of a library of aroyl hydrazones based on benzothiazole skeleton. All the compounds of the developed library are characterized by various spectral techniques. α-Amylase inhibitory potential of all compounds has been explored, where compound **7n** exhibits remarkable α-amylase inhibition of 87.5% at 50 µg/mL. Robust QSAR models are made by using the balance of correlation method in CORAL software. The chemical structures at different concentration with optimal descriptors are represented by SMILES. A data set of 66 SMILES of 22 hydrazones at three distinct concentrations are prepared. The significance of the index of ideality of correlation (IIC) with applicability domain (AD) is also studied at depth. A QSAR model with best $R^2_{validation} = 0.8587$ for split 1 is considered as a leading model. The outliers and promoters of increase and decrease of endpoint are also extracted. The binding modes of the most active compound, that is, **7n** in the active site of *Aspergillus oryzae* α-amylase (**PDB ID: 7TAA**) are also explored by *in silico* molecular docking studies. Compound **7n** displays high resemblance in binding mode and pose with the standard drug acarbose. Molecular dynamics simulations performed on protein–ligand complex for 100 ns, the protein gets stabilised after 20 ns and remained below 2 Å for the remaining simulation. Moreover, the deviation observed in RMSF during simulation for each amino acid residue with respect to Cα carbon atom is insignificant.

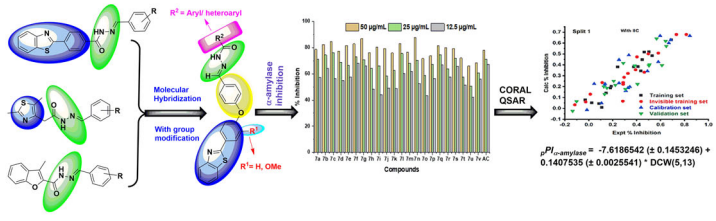

ARTICLE HISTORY
Received 12 August 2020
Accepted 9 December 2020

KEYWORDS
Benzothiazole; aroyl hydrazone; α-amylase inhibition; molecular docking; QSAR; IIC

Abbreviations: IIC: index of ideality of correlation; CW: correlation weight; OECD: Organization of Economic Co-operation and Development; QSAR: quantitative structure–activity relationship; CORAL: CORrelation And Logic; AD: applicability domain; MD: molecular dynamics

1. Introduction

Diabetes and obesity are a cluster of metabolic disorders related to lifestyle and characterised by high blood glucose over a prolonged time. The increasing occurrence of these two disorders accelerated the discovery of new drugs. α-Amylase (EC 3.2.1.1) is an endoamylase which mainly occurs in plants, microorganism and higher organisms and belongs to 13th family of glycoside hydrolases (GH13). Its main function is to hydrolyze the α-D-(1,4)-glycosidic linkage in starch (Brayer et al., 1995; Shi et al., 2018; Souza & Magalhães, 2010) and retaining α-anomeric configuration in the products. The over-expression of α-amylase leads to hyperglycaemia which results in the development of diabetes mellitus. This feature established α-amylase as a well-known molecular target for type 2 diabetes mellitus. Marketed drugs prescribed to treat type-II diabetes mellitus are associated with numerous side effects such as diarrhoea,

CONTACT Parvin Kumar parvinjangra@gmail.com; parvinchem@kuk.ac.in Department of Chemistry, Kurukshetra University, Kurukshetra, India
Supplemental data for this article can be accessed online at https://doi.org/10.1080/07391102.2020.1863861.

abdominal discomfort and flatulence. Therefore, there is a strong need to develop new drugs with lesser side effect and better selectivity.

In recent years, *N* and *S* containing heterocyclic compounds have attracted synthetic medicinal chemist owing to their numerous pharmacological properties. 1,3-Benzothiazole is one of the important *N*- and *S*-containing heterocyclic scaffold which has gained the attention due to its use in a wide range of industrial (Kaur et al., 2018; Sharma et al., 2018) and biological applications (Bhutani et al., 2018; Gollapalli et al., 2019; Kumar et al., 2017c; Mishra et al., 2019; Murtuja et al., 2018). Similarly, aroyl hydrazone has acquired a leading position in the pharmacophoric framework of biologically active compounds (Angelova et al., 2016; Cardoso et al., 2017; Hernández-Vázquez et al., 2016; Kumar et al., 2017b; Thota et al., 2018).

Quantitative structure–activity relationship (QSAR) is an important technique for predicting the biological effects of molecules based on mathematical and statistical relationship (Krallinger et al., 2017; Le et al., 2012). CORAL software (http://www.insilico.eu/CORAL) is a user-friendly freely available software and has been used to develop QSAR models for various endpoints (Kumar & Chauhan, 2017; Kumar et al., 2019c; Toropova & Toropov et al., 2019a). The optimal descriptors, so-called correlation weights, are calculated from SMILES using the Monte Carlo optimization method where correlation coefficient between the endpoint and optimal descriptor are used to compute the target function. Literature survey reveals that the index of ideality of correlation (IIC) has been applied to validate the developed QSAR models (Toropov & Toropova, 2019; Toropov et al., 2019; Toropova & Toropov, 2019b, 2019c). The IIC evaluates the predictive capability of the QSAR model, which is not only concerned with the correlation coefficient but to the residual values of the endpoint and dot alignment of the image relative to the diagonal (Toropova & Toropov, 2019b, 2019c).

To the best of our knowledge, there is no scientific report on benzothiazole clubbed hydrazone as α-amylase inhibitors. Continuing our ongoing research on *N/S* containing heterocyclic compounds (Bhatia et al., 2019; Kumar et al., 2017a, 2018) and in search of novel therapeutic agents, we, herein report the synthesis and α-amylase inhibitory potential of novel molecular hybrids of benzothiazole clubbed hydrazone with QSAR study. The objectives of the present study are: (i) Multistep synthesis of benzothiazole clubbed with hydrazone *via* ether linkage (**7a**–**7v**) and *in vitro* α-amylase inhibition at three different concentrations (50, 25, 12.5 μg/mL); (ii) Building up and estimation of QSAR models using Monte Carlo approach with IIC; (iii) Extraction of structural features responsible for the increase and decrease of α-amylase inhibition and (iv) Docking studies to explore the probable binding modes.

2. Results and discussion

2.1. Design and development of α-amylase inhibitors

Based on the activity reported in the literature (Taha et al., 2015, 2017, 2019), we have designed a series of new α-amylase inhibitors (Figure 1). Taha et al. recently reported hydrazones as α-amylase and α-glucosidase inhibitors with a wide range of IC_{50} value (Taha et al., 2015, 2017, 2019). The presence of a thiazole, benzofuran and benzothiazole on one side of hydrazone played an important role in the inhibition of target. The effect of different substituents on the phenyl ring of carbaldehyde was also investigated by the authors. Using these tactics, we have designed and prepared a series of new derivatives of benzothiazole linked with hydrazone *via* an ether linkage. Further, we focused on optimizing the aryl/heteroaryl region of the imine group and phenyl ring of the ether linkage.

2.2. Synthesis of α-amylase inhibitors

The synthetic sequence of (*E*)-*N*′-(4-(4-(benzo[*d*]thiazol-2-yl)aryloxy)benzylidene)-(aryl)hydrazide (**7a**–**7v**) is presented in Scheme 2. The key intermediate, 4-(4-(benzo[*d*]thiazol-2-yl)aryloxy)benzaldehyde (**5a**–**5b**) was prepared in two steps from the commercially available 2-aminothiophenol (**1**) (1.00 mmol), *p*-hydroxybenzaldehyde (**2a**) (1.00 mmol)/vanillin (**2b**) (1.00 mmol) and 4-fluorobenzaldehyde (**4**) (1.00 mmol). The SiO_2 supported HNO_3 catalysed condensation of 2-aminothiophenol (**1**) (1.00 mmol) with *p*-hydroxybenzaldehyde (**2a**) (1.00 mmol)/vanillin (**2b**) (1.00 mmol) under the solvent-free condition at room temperature resulted in the formation of 2-arylbenzothiazole (**3a–3b**) (Kumar et al., 2015). Further, compound **3** was arylated with *p*-fluorobenzaldehyde (**4**) (1.00 mmol) using K_2CO_3 (1.20 mmol) in dimethyl sulfoxide (DMSO) at 120 °C for 4–5 h. The reaction resulted in the formation of 4-(4-(benzo[*d*]thiazol-2-yl)aryloxy) benzaldehyde (**5a–5b**) in 90% yield and confirmed by spectral analysis (Scheme 1).

A condensation reaction of 4-(4-(benzo[*d*]thiazol-2-yl)aryloxy)benzaldehyde (**5a–5b**) was attempted with corresponding aryl/heteroaryl hydrazide (**6a–6k**) in refluxing EtOH:THF (4:1; 20 mL) using a catalytic amount of acetic acid. All the reaction proceeded smoothly and afforded *N*′-(4-(4-(benzo[*d*]-thiazol-2-yl)aryloxy)benzylidene)-(aryl)hydrazides (**7a–7v**) in 79–90% yield (Scheme 2, Table 1). The structure of all the compounds (**7a–7v**) were confirmed by spectral analysis, that is, IR, ^{1}H NMR, ^{13}C NMR and elemental analysis (Figures S1–S49).

2.3. Spectral characterization

In the IR spectra of compounds **7a–7v**, absorption signals corresponding to N–H and C = O stretching appeared at 3435–3209 cm^{-1} and 1660–1638 cm^{-1}, respectively. In the case of compound **7f**, the appearance of a singlet at δ 11.82 ppm in the ^{1}H NMR spectrum confirmed the presence of amidic –N**H**–. In addition to this, the appearance of two singlets at δ 8.48 ppm and 2.39 ppm revealed the presence of imine [–N = C**H**–(H_{23})] and methyl (–C$\mathbf{H}_3$) groups, respectively. All the aromatic protons resonate in the region of δ 8.16–7.21 ppm. A doublet appeared at δ 7.35 ppm (J = 8.0 Hz) corresponding to H_{29}/H_{31} protons showed a correlation with protons H_{28}/H_{32} resonating at δ 7.83 (J = 12.1, 8.4 Hz) appears

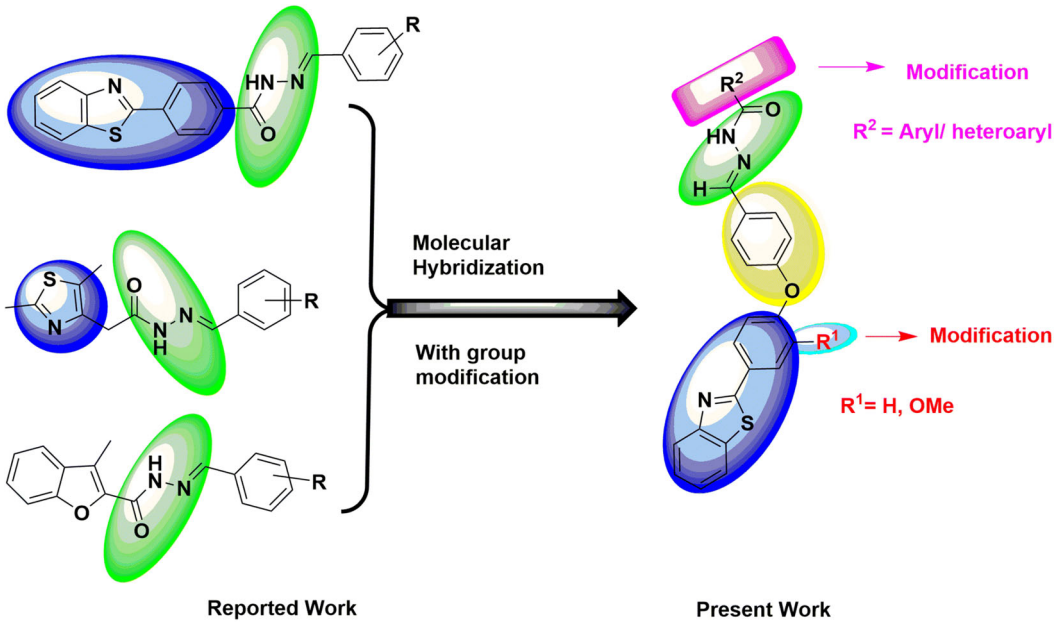

Figure 1. Designing of target compounds as α-amylase inhibitors.

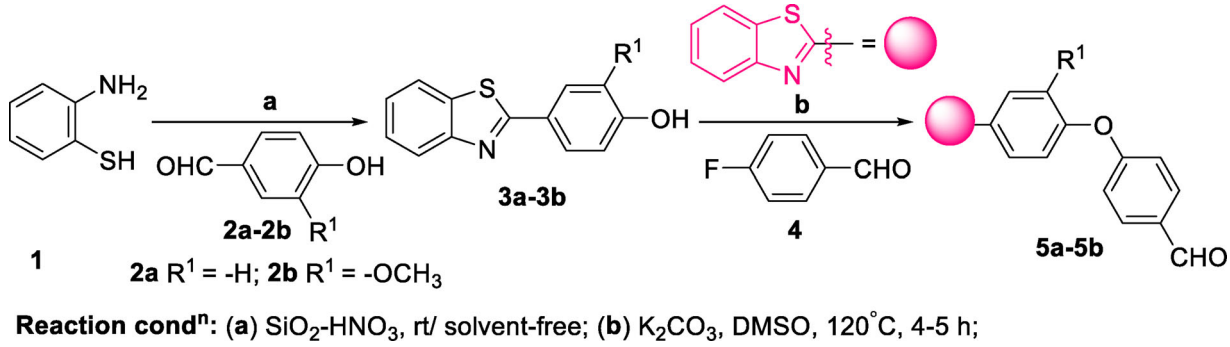

Scheme 1. Synthesis of 4-(4-(benzo[*d*]thiazol-2-yl)aryloxy)benzaldehydes (**5a–5b**).

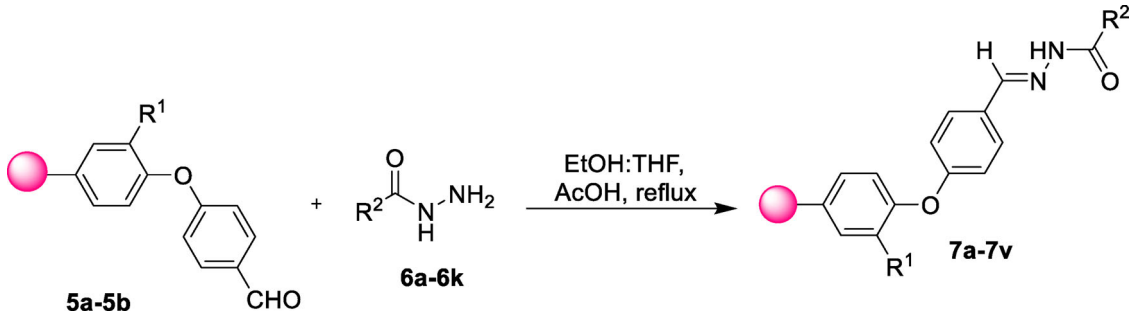

Scheme 2. Synthesis of benzothiazole clubbed hydrazone (**7a–7v**) based molecular hybrids.

in the form of a doublet of doublet. A multiplet at δ 8.16–8.14 ppm corresponds to H_{11}/H_{15} protons showed a correlation with protons H_{12}/H_{14} resonating in the form of the triplet at δ 7.23 ppm ($J = 8.6$ Hz). H_5 proton resonating at δ 8.16–8.14 ppm in the form of multiplet showed a correlation with proton H_6 resonating at δ 7.49–7.45 ppm in the form of the multiplet. A doublet at δ 8.06 ($J = 7.7$ Hz) corresponds to H_8 proton showed a correlation with proton H_7 appeared in the form of multiplet at δ 7.57–7.53 ppm. Proton H_{19}/H_{21} resonating at δ 7.83 ($J = 12.1$, 8.4 Hz) in the form doublet of doublet showed a correlation with proton H_{18}/H_{12} present in the form of the triplet at δ 7.23 ($J = 8.6$ Hz) as shown in Figure 2.

The proton decoupled ^{13}C NMR of compound **7f** showed 24 peaks, in which signal at δ 21.0 ppm corresponds to C**H**$_3$ proton. A singlet at δ 2.42 ppm due to three protons

confirms the presence of the methyl (–C**H**$_3$) group. A doublet at δ 8.07 ppm ($J = 7.85$ Hz) corresponds to H_8 proton showed a correlation with proton H_7 present at δ 7.58–7.54 ppm in the form of the multiplet. A doublet at δ 8.03 ppm ($J = 8.19$ Hz) corresponds to H_{29}/H_{33} proton showed a correlation with proton H_{30}/H_{32} present at δ 7.49–7.45 ppm in the form of the multiplet. A doublet at δ 7.36 ppm ($J = 8.75$ Hz) and 7.32 ppm ($J = 8.19$ Hz) for protons H_{18}/H_{22} and H_{12}/H_{14} showed a correlation with proton present at δ 8.21–8.15 ppm for H_{19}/H_{21} and H_{11}/H_{15} in the form of the multiplet. The aromatic resonates from δ 8.22 to7.30 ppm, as shown in Figure 2. In the ESI-MS mass spectra of compound **7f** the *m/z* value was observed at 464.1424 ($m + 1$), respectively.

2.4. Biological studies

Continuing our efforts towards the development of novel α-amylase inhibitors (Duhan et al., 2019; Kumar et al., 2017a), we screened all the synthesised compounds for inhibitory potential of α-amylase at three different concentrations (50, 25, 12.5 μg/mL) as shown in Table 2. The inhibitory potential of all the compounds was also compared with standard drug acarbose. The selectivity and inhibitory activity profile related to the different heteroaryl ring and functional group in compounds **7a–7v** have also been studied.

The maximum inhibition potential at 50 μg/mL, 25 μg/mL and 12.5 μg/mL were displayed by compounds **7n**, **7c** and **7f**, respectively. Compound **7n** was found to be the most potent with 87.5% of inhibition at 50 μg/mL. As far as minimum inhibition potential is concerned, among hydrazones, compound **7u** exhibited the lowest inhibitory activity at all concentrations, that is, 50 μg/mL (65.99%), 25 μg/mL (50.74%) and 12.5 μg/mL (42.28%) (Table 2). A comparative graph of % inhibition for compounds **7a–7v** with standard drug acarbose is shown in Figure 3.

Table 1. Synthesis of benzothiazole clubbed hydrazone (**7a–7v**) based molecular hybrids.

S. no.	–R1	–R2	Compounds	Yield (%)
1.	–H	–C_6H_5	**7a**	84
2.	–H	4-NO_2–C_6H_4	**7b**	88
3.	–H	4-Cl–C_6H_4	**7c**	87
4.	–H	4-Pyridyl	**7d**	80
5.	–H	4-OCH_3–C_6H_4	**7e**	88
6.	–H	4-CH_3–C_6H_4	**7f**	90
7.	–H	4-Br–C_6H_4	**7g**	89
8.	–H	3-Pyridyl	**7h**	80
9.	–H	2-Furyl	**7i**	81
10.	–H	2-Thenyl	**7j**	83
11.	–H	3-CH_3–C_6H_4	**7k**	85
12.	–OCH_3	–C_6H_5	**7l**	83
13.	–OCH_3	4-NO_2–C_6H_4	**7m**	87
14.	–OCH_3	4-Cl–C_6H_4	**7n**	85
15.	–OCH_3	4-Pyridyl	**7o**	79
16.	–OCH_3	4-OCH_3–C_6H_4	**7p**	87
17.	–OCH_3	4-CH_3–C_6H_4	**7q**	89
18.	–OCH_3	4-Br–C_6H_4	**7r**	83
19.	–OCH_3	3-Pyridyl	**7s**	81
20.	–OCH_3	2-Furyl	**7t**	78
21.	–OCH_3	2-Thenyl	**7u**	80
22.	–OCH_3	3-CH_3–C_6H_4	**7v**	88

3. QSAR studies

3.1. Data set for QSAR

QSAR/QSPR is a significant method to establish a link between the structure and endpoint of the compounds (Karelson et al., 1996). To find out the most contributing molecular structure from the studied hydrazones as α-amylase inhibitors, QSAR models were developed using CORAL software. Data set for Hydrazones (Table 3) with their % inhibition at three different concentrations (50 μg/mL, 25 μg/mL and 12.5 μg/mL) were selected for the generation of QSAR models. Chemical structures of 22 newly synthesized compounds (**7a–7v**) were sketched using ChemAxon software (Version & 6.2.2, 2014) and SMILES were generated from those. The symbols $, % and & are used as quasi-SMILES notation for three different concentrations, that is, 50 μg/mL, 25 μg/mL and 12.5 μg/mL. The present data set of 66 SMILES comprising of both standard SMILES and quasi-SMILES notation, in which standard SMILES has been used before quasi SMILES. Four random splits were made. The non-identical nature (Kumar et al., 2019c; Toropova et al., 2017) of these splits were calculated using the reported

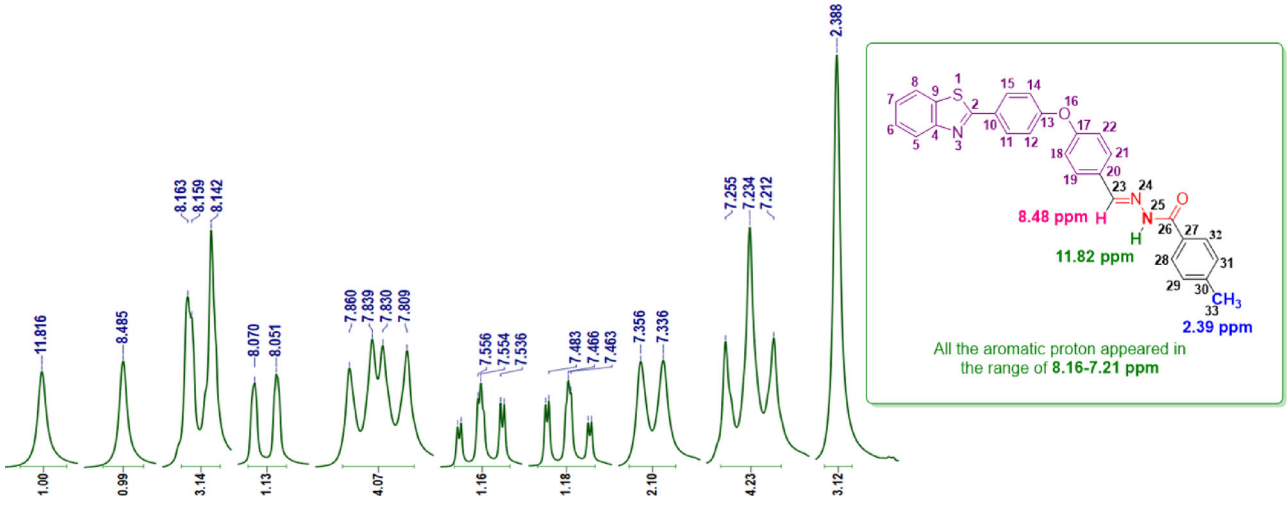

Figure 2. Various characteristic peaks of compound **7f**.

methodology (Table S1) (see Supplementary Information). Each split was further divided into four sets having individual responsibility such as (i) *Training set*: was used to prepare the QSAR model by computing the correlation weights (CW); (ii) *Invisible-training set*: was responsible for checking the fitness of the compounds which were absent in training set; (iii) *Calibration set*: used to identify the start of overtraining and (iv) *Validation sets*: used to validate the QSAR models (Achary et al., 2019; Kumar et al., 2019b). The percentage inhibition activity of α-amylase is expressed in logarithmic scale using the following equation

$$pPI_{\alpha-amylase} = -\log\left(\frac{100-PI_{\alpha-amylase}}{PI_{\alpha-amylase}}\right) \quad (1)$$

Here, $PI_{\alpha-amylase}$ stands for the percentage inhibition of α-amylase at various concentrations.

Table 2. α-Amylase inhibition activity of (*E*)-*N*′-(4-(4-(benzo[*d*]thiazol-2-yl)aryloxy)benzylidene)-(aryl)hydrazides (**7a–7v**).

		% Inhibition		
		Concentration (μg/mL)		
S. no.	Compound	50	25	12.5
1	**7a**	78.68 ± 1.98	71.14 ± 1.85	57.17 ± 1.63
2	**7b**	82.35 ± 1.87	74.45 ± 1.71	64.15 ± 1.49
3	**7c**	84.38 ± 1.73	76.10 ± 1.54	56.43 ± 1.13
4	**7d**	77.21 ± 1.82	68.75 ± 1.80	54.96 ± 1.47
5	**7e**	81.62 ± 1.92	66.36 ± 1.58	57.54 ± 1.57
6	**7f**	82.9 ± 1.62	73.16 ± 1.55	68.03 ± 1.33
7	**7g**	86.76 ± 1.88	70.77 ± 1.38	65.99 ± 1.61
8	**7h**	76.10 ± 1.96	64.15 ± 1.80	48.35 ± 1.25
9	**7i**	80.33 ± 1.80	65.99 ± 1.76	44.12 ± 1.21
10	**7j**	79.23 ± 1.85	58.27 ± 1.41	49.08 ± 1.14
11	**7k**	75.92 ± 1.57	62.50 ± 1.37	48.53 ± 1.01
12	**7l**	83.09 ± 1.89	75.55 ± 1.98	60.29 ± 1.73
13	**7m**	76.29 ± 1.86	68.01 ± 1.74	61.76 ± 1.75
14	**7n**	87.50 ± 1.09	70.40 ± 1.04	52.57 ± 1.11
15	**7o**	71.69 ± 1.69	58.64 ± 1.24	43.38 ± 1.03
16	**7p**	73.71 ± 1.45	67.10 ± 1.51	56.25 ± 1.10
17	**7q**	81.43 ± 1.40	74.45 ± 1.45	66.91 ± 1.14
18	**7r**	79.78 ± 1.64	63.60 ± 1.53	57.72 ± 1.20
19	**7s**	79.23 ± 1.52	71.87 ± 1.41	65.81 ± 1.25
20	**7t**	72.06 ± 1.74	57.54 ± 1.25	51.47 ± 1.23
21	**7u**	65.99 ± 1.94	50.74 ± 1.29	42.28 ± 1.25
22	**7v**	68.38 ± 1.80	60.66 ± 1.75	56.07 ± 1.47
23	**Acarbose (AC)**	77.96 ± 1.63	71.17 ± 1.74	67.25 ± 1.39

3.2. QSAR building

The data set of 66 SMILES of 22 compounds at three different concentrations was made to develop QSAR model. A detailed explanation of the SMILES features is shown in Table 4.

The dataset was further divided into four random splits (Table 5). Four sets, that is, training, invisible training, calibration and validation sets were made from each split. The prediction of a developed QSAR model was also assessed in the context of IIC. To check the robustness and predictability of the constructed QSAR models, various statistical parameters (Kumar & Kumar, 2020) such as R^2, CCC, IIC, Q^2 (cross-validated correlation coefficient), *s*, MAE, *F*, $C_{R_p^2}$, *Y*-test, RMSEP, Q^2F_1, Q^2F_2, Q^2F_3 and R^2m (avg) were calculated and these parameters are depicted in Table 5. By using the equation of $\mathbf{TF_1}$ for splits 1, 2, 3 and 4, the best (T^*, N^*) are (6, 7), (2, 8), (1, 7), (5, 5). However, by considering the influence of IIC on the activity ($pPI_{\alpha-amylase}$), the equation of $\mathbf{TF_2}$ for splits 1, 2, 3 and 4 resulted into different (T^*, N^*) and these are (5, 13), (6, 13), (5, 17) and (3, 16). The above outcome clearly shows that the preferable threshold and number of epochs for both target functions are not identical. A total of eight QSAR models was built using the balance of correlation method with IIC (four for each data set using $\mathbf{TF_2}$) and without IIC (four for each data set using $\mathbf{TF_1}$). The IIC was also implemented to improve the predictability and robustness of developed QSAR models. The best QSAR models, along with other statistical parameters, are presented in Table 5. The values of these statistical parameters are a good sign of the robust QSAR models. The value of $\boldsymbol{R^2 = 0.8587}$ was highest for the validation set of split 1 using IIC, so this QSAR model was

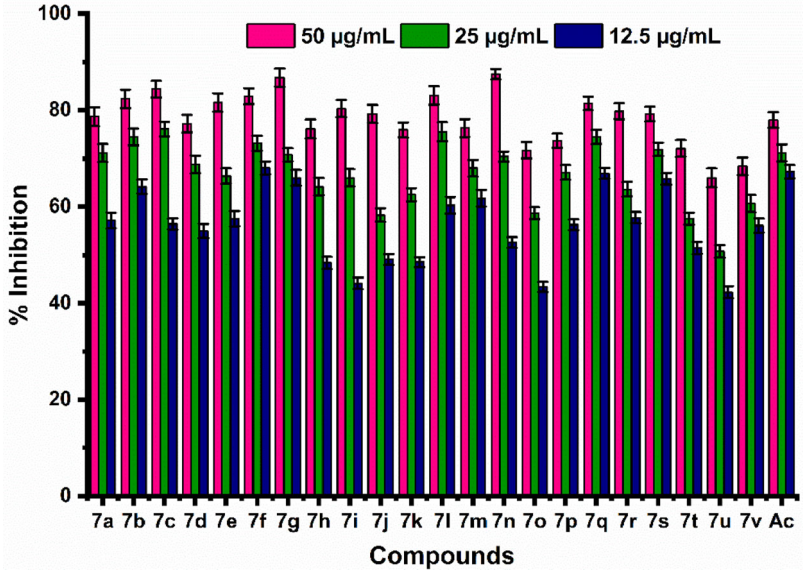

Figure 3. Comparative analysis of percentage inhibition of compounds **7a–7v**.

Table 3. Split distribution with SMILES notation at different concentration, experimental, calculated, residual $pPI_{\alpha-amylase}$ % with applicability domain (AD) using TF_2 (with IIC) for compounds (**7a–7v**).

Splits								Experimental[a]	Calculated $pPI_{\alpha-amylase}$ for each splits				Residual $pPI_{\alpha-amylase}$ for each splits				Applicability domain			
1	2	3	4	Compounds	ID	SMILES	$pPI_{\alpha-amylase}$	Split 1	Split 2	Split 3	Split 4	Split 1	Split 2	Split 3	Split 4	Split 1	Split 2	Split 3	Split 4
+	−	#	*	**7a**	HYD01	N(/N = C\c1ccc(Oc2ccc(cc2)c2nc3ccccc3s2)cc1)C(=O)c1ccccc1$	0.5671	0.6350	0.7505	0.6951	0.6408	−0.0679	−0.1835	−0.1281	−0.0737	YES	YES	YES	YES
−	+	*	#	**7b**	HYD02	N(/N = C\c1ccc(Oc2ccc(cc2)c2nc3ccccc3s2)cc1)C(=O)c1ccc(cc1)[N+](=O)[O-]$	0.6689	0.5549	0.6795	0.5116	0.5999	0.1140	−0.0105	0.1573	0.0690	YES	YES	YES	YES
#	*	+	−	**7c**	HYD03	N(/N = C\c1ccc(Oc2ccc(cc2)c2nc3ccccc3s2)cc1)C(=O)c1ccc(Cl)cc1$	0.7326	0.7011	0.7311	0.7150	0.6790	0.0315	0.0015	0.0180	0.0536	YES	YES	YES	YES
*	#	−	+	**7d**	HYD04	N(/N = C\c1ccc(Oc2ccc(cc2)c2nc3ccccc3s2)cc1)C(=O)c1ccncc1$	0.5299	0.6326	0.5781	0.5831	0.4852	−0.1027	−0.0481	−0.0531	0.0447	YES	YES	YES	No
+	−	#	*	**7e**	HYD05	N(/N = C\c1ccc(Oc2ccc(cc2)c2nc3ccccc3s2)cc1)C(=O)c1ccc(OC)cc1$	0.6475	0.6452	0.5879	0.6282	0.5718	0.0023	0.0591	0.0188	0.0757	YES	YES	YES	YES
−	+	*	#	**7f**	HYD06	N(/N = C\c1ccc(Oc2ccc(cc2)c2nc3ccccc3s2)cc1)C(=O)c1ccc(C)cc1$	0.6856	0.7039	0.7326	0.6778	0.6302	−0.0183	−0.0466	0.0078	0.0554	YES	YES	YES	YES
#	*	+	−	**7g**	HYD07	N(/N = C\c1ccc(Oc2ccc(cc2)c2nc3ccccc3s2)cc1)C(=O)c1ccc(Br)cc1$	0.8164	0.7011	0.7311	0.7150	0.6790	0.1153	0.0853	0.1010	0.1374	YES	YES	YES	YES
*	#	−	+	**7h**	HYD08	N(/N = C\c1ccc(Oc2ccc(cc2)c2nc3ccccc3s2)cc1)C(=O)c1cccnc1$	0.5030	0.5870	0.5856	0.5832	0.5199	−0.0840	−0.0826	−0.0802	−0.0169	YES	YES	YES	YES
+	−	#	*	**7i**	HYD09	N(/N = C\c1ccc(Oc2ccc(cc2)c2nc3ccccc3s2)cc1)C(=O)c1ccco1$	0.6111	0.4686	0.4275	0.4014	0.3955	0.1425	0.1835	0.2096	0.2156	YES	YES	YES	YES
−	+	*	#	**7j**	HYD10	N(/N = C\c1ccc(Oc2ccc(cc2)c2nc3ccccc3s2)cc1)C(=O)c1ccsc1$	0.5815	0.4211	0.4691	0.3616	0.4282	0.1604	0.1129	0.2199	0.1533	YES	YES	YES	YES
#	*	+	−	**7k**	HYD11	N(/N = C\c1ccc(Oc2ccc(cc2)c2nc3ccccc3s2)cc1)C(=O)c1cccc(C)c1$	0.4987	0.5457	0.6026	0.5576	0.5009	−0.0470	−0.1039	−0.0586	−0.0022	YES	YES	YES	YES
*	#	−	+	**7l**	HYD12	N(/N = C\c1ccc(Oc2ccc(cc2OC)c2nc3ccccc3s2)cc1)C(=O)c1ccccc1$	0.6914	0.5691	0.6827	0.6579	0.6293	0.1223	0.0083	0.0331	0.0621	YES	YES	YES	YES
+	−	#	*	**7m**	HYD13	N(/N = C\c1ccc(Oc2ccc(cc2OC)c2nc3ccccc3s2)cc1)C(=O)c1ccc(cc1)[N+](=O)[O-]$	0.5075	0.5112	0.6552	0.4858	0.4043	−0.0037	−0.1482	0.0212	0.1032	YES	YES	YES	YES
−	+	*	#	**7n**	HYD14	N(/N = C\c1ccc(Oc2ccc(cc2OC)c2nc3ccccc3s2)cc1)C(=O)c1ccc(Cl)cc1$	0.8451	0.6352	0.6633	0.6778	0.6675	0.2099	0.1817	0.1673	0.1776	YES	YES	YES	YES
#	*	+	−	**7o**	HYD15	N(/N = C\c1ccc(Oc2ccc(cc2OC)c2nc3ccccc3s2)cc1)C(=O)c1ccncc1$	0.4035	0.5667	0.5102	0.5458	0.4738	−0.1632	−0.1067	−0.1418	−0.0703	YES	YES	YES	No
*	#	−	+	**7p**	HYD16	N(/N = C\c1ccc(Oc2ccc(cc2OC)c2nc3ccccc3s2)cc1)C(=O)c1ccc(OC)cc1$	0.4477	0.5395	0.4679	0.5081	0.4495	−0.0918	−0.0199	−0.0601	−0.0018	YES	YES	YES	YES
+	−	#	*	**7q**	HYD17	N(/N = C\c1ccc(Oc2ccc(cc2OC)c2nc3ccccc3s2)cc1)C(=O)c1ccc(C)cc1$	0.6420	0.6380	0.6648	0.6406	0.6187	0.0040	−0.0228	0.0014	0.0233	YES	YES	YES	YES
−	+	*	#	**7r**	HYD18	N(/N = C\c1ccc(Oc2ccc(cc2OC)c2nc3ccccc3s2)cc1)C(=O)c1ccc(Br)cc1$	0.5961	0.6352	0.6633	0.6778	0.6675	−0.0391	−0.0673	−0.0817	−0.0714	YES	YES	YES	YES
#	*	+	−	**7s**	HYD19	N(/N = C\c1ccc(Oc2ccc(cc2OC)c2nc3ccccc3s2)cc1)C(=O)c1cccnc1$	0.5815	0.5212	0.5178	0.5460	0.5085	0.0603	0.0637	0.0360	0.0730	YES	YES	YES	YES
*	#	−	+	**7t**	HYD20	N(/N = C\c1ccc(Oc2ccc(cc2OC)c2nc3ccccc3s2)cc1)C(=O)c1ccco1$	0.4115	0.4027	0.3597	0.3642	0.3840	0.0088	0.0513	0.0468	0.0275	YES	YES	YES	YES
+	−	#	*	**7u**	HYD21	N(/N = C\c1ccc(Oc2ccc(cc2OC)c2nc3ccccc3s2)cc1)C(=O)c1ccsc1$	0.2879	0.3552	0.4012	0.3244	0.4167	−0.0673	−0.1132	−0.0364	−0.1288	YES	YES	YES	YES
−	+	*	#	**7v**	HYD22	N(/N = C\c1ccc(Oc2ccc(cc2OC)c2nc3ccccc3s2)cc1)C(=O)c1cccc(C)c1$	0.3350	0.4799	0.5348	0.5204	0.4894	−0.1449	−0.1998	−0.1854	−0.1544	YES	YES	YES	YES
#	*	+	−	**7a**	HYD23	N(/N = C\c1ccc(Oc2ccc(cc2)c2nc3ccccc3s2)cc1)C(=O)c1ccccc1%	0.3918	0.3700	0.4776	0.4122	0.3545	0.0218	−0.0858	−0.0202	0.0373	YES	YES	YES	YES
*	#	−	+	**7b**	HYD24	N(/N = C\c1ccc(Oc2ccc(cc2)c2nc3ccccc3s2)cc1)C(=O)c1ccc(cc1)[N+](=O)[O-]%	0.4645	0.4237	0.4065	0.4070	0.5173	0.0408	0.0585	0.0580	−0.0528	YES	YES	YES	YES
+	−	#	*	**7c**	HYD25	N(/N = C\c1ccc(Oc2ccc(cc2)c2nc3ccccc3s2)cc1)C(=O)c1ccc(Cl)cc1%	0.5030	0.4360	0.4582	0.4321	0.3926	0.0670	0.0448	0.0709	0.1104	YES	YES	YES	YES
−	+	*	#	**7d**	HYD26	N(/N = C\c1ccc(Oc2ccc(cc2)c2nc3ccccc3s2)cc1)C(=O)c1ccncc1%	0.3424	0.3675	0.3051	0.3001	0.1989	−0.0251	0.0369	0.0423	0.1435	YES	YES	YES	No
#	*	+	−	**7e**	HYD27	N(/N = C\c1ccc(Oc2ccc(cc2)c2nc3ccccc3s2)cc1)C(=O)c1ccc(OC)cc1%	0.2951	0.3802	0.3149	0.3453	0.2855	−0.0851	−0.0198	−0.0503	0.0096	YES	YES	YES	YES
*	#	−	+	**7f**	HYD28	N(/N = C\c1ccc(Oc2ccc(cc2)c2nc3ccccc3s2)cc1)C(=O)c1ccc(C)cc1%	0.4355	0.4388	0.4597	0.3949	0.3439	−0.0033	−0.0237	0.0411	0.0916	YES	YES	YES	YES
+	−	#	*	**7g**	HYD29	N(/N = C\c1ccc(Oc2ccc(cc2)c2nc3ccccc3s2)cc1)C(=O)c1ccc(Br)cc1%	0.3840	0.4360	0.4582	0.4321	0.3926	−0.0520	−0.0742	−0.0481	−0.0086	YES	YES	YES	YES
−	+	*	#	**7h**	HYD30	N(/N = C\c1ccc(Oc2ccc(cc2)c2nc3ccccc3s2)cc1)C(=O)c1cccnc1%	0.2527	0.3220	0.3127	0.3003	0.2336	−0.0693	−0.0597	−0.0476	0.0191	YES	YES	YES	YES
#	*	+	−	**7i**	HYD31	N(/N = C\c1ccc(Oc2ccc(cc2)c2nc3ccccc3s2)cc1)C(=O)c1ccco1%	0.2879	0.1626	0.1545	0.2146	0.2219	0.1253	0.1334	0.0734	0.0660	YES	YES	YES	YES
*	#	−	+	**7j**	HYD32	N(/N = C\c1ccc(Oc2ccc(cc2)c2nc3ccccc3s2)cc1)C(=O)c1ccsc1%	0.1450	0.1560	0.1961	0.0787	0.1419	−0.0110	−0.0511	0.0663	0.0031	YES	YES	YES	YES
+	−	#	*	**7k**	HYD33	N(/N = C\c1ccc(Oc2ccc(cc2)c2nc3ccccc3s2)cc1)C(=O)c1cccc(C)c1%	0.2218	0.2807	0.3296	0.2747	0.2146	−0.0589	−0.1076	−0.0527	0.0072	YES	YES	YES	YES
−	+	*	#	**7l**	HYD34	N(/N = C\c1ccc(Oc2ccc(cc2OC)c2nc3ccccc3s2)cc1)C(=O)c1ccccc1%	0.4900	0.3041	0.4098	0.3749	0.3430	0.1859	0.0802	0.1151	0.1470	YES	YES	YES	YES
#	*	+	−	**7m**	HYD35		0.3276	0.3800	0.3822	0.3812	0.3216	−0.0524	−0.0546	−0.0532	0.0060	YES	YES	YES	YES

(*continued*)

Table 3. Continued.

Splits							Experimental[a]	Calculated $pPI_{\alpha-amylase}$ for each splits				Residual $pPI_{\alpha-amylase}$ for each splits				Applicability domain			
1	2	3	4	Compounds	ID	SMILES	$pPI_{\alpha-amylase}$	Split 1	Split 2	Split 3	Split 4	Split 1	Split 2	Split 3	Split 4	Split 1	Split 2	Split 3	Split 4
						N(/N = C\c1ccc(Oc2ccc(cc2OC)c2nc3ccccc3s2)cc1)C(=O)c1ccc(cc1)[N+](=O)[O-]%													
*	#	−	+	**7n**	HYD36	N(/N = C\c1ccc(Oc2ccc(cc2OC)c2nc3ccccc3s2)cc1)C(=O)c1ccc(Cl)cc1%	0.3763	0.3702	0.3903	0.3949	0.3812	0.0061	−0.0143	−0.0189	−0.0049	YES	YES	YES	YES
+	−	#	*	**7o**	HYD37	N(/N = C\c1ccc(Oc2ccc(cc2OC)c2nc3ccccc3s2)cc1)C(=O)c1ccncc1%	0.1516	0.3017	0.2373	0.2629	0.1875	−0.1501	−0.0853	−0.1109	−0.0359	YES	YES	YES	No
−	+	*	#	**7p**	HYD38	N(/N = C\c1ccc(Oc2ccc(cc2OC)c2nc3ccccc3s2)cc1)C(=O)c1ccc(OC)cc1%	0.3095	0.2745	0.1949	0.2252	0.1632	0.0350	0.1151	0.0843	0.1463	YES	YES	YES	YES
#	*	+	−	**7q**	HYD39	N(/N = C\c1ccc(Oc2ccc(cc2OC)c2nc3ccccc3s2)cc1)C(=O)c1ccc(C)cc1%	0.4645	0.3729	0.3918	0.3576	0.3324	0.0916	0.0727	0.1074	0.1321	YES	YES	YES	YES
*	#	−	+	**7r**	HYD40	N(/N = C\c1ccc(Oc2ccc(cc2OC)c2nc3ccccc3s2)cc1)C(=O)c1ccc(Br)cc1%	0.2424	0.3702	0.3903	0.3949	0.3812	−0.1278	−0.1483	−0.1529	−0.1388	YES	YES	YES	YES
+	−	#	*	**7s**	HYD41	N(/N = C\c1ccc(Oc2ccc(cc2OC)c2nc3ccccc3s2)cc1)C(=O)c1cccnc1%	0.4074	0.2561	0.2449	0.2631	0.2222	0.1513	0.1621	0.1439	0.1852	YES	YES	YES	No
−	+	*	#	**7t**	HYD42	N(/N = C\c1ccc(Oc2ccc(cc2OC)c2nc3ccccc3s2)cc1)C(=O)c1ccco1%	0.1320	0.0967	0.0867	0.1774	0.2104	0.0353	0.0453	−0.0454	−0.0784	YES	YES	YES	YES
#	*	+	−	**7u**	HYD43	N(/N = C\c1ccc(Oc2ccc(cc2OC)c2nc3ccccc3s2)cc1)C(=O)c1ccsc1%	0.0129	0.0902	0.1283	0.0415	0.1304	−0.0773	−0.1154	−0.0285	−0.1175	YES	YES	YES	YES
*	#	−	+	**7v**	HYD44	N(/N = C\c1ccc(Oc2ccc(cc2OC)c2nc3ccccc3s2)cc1)C(=O)c1cccc(C)c1%	0.1881	0.2148	0.2618	0.2374	0.2031	−0.0267	−0.0738	−0.0494	−0.0150	YES	YES	YES	YES
+	−	#	*	**7a**	HYD45	N(/N = C\c1ccc(Oc2ccc(cc2)c2nc3ccccc3s2)cc1)C(=O)c1ccccc1&	0.1254	0.1407	0.3000	0.1842	0.1997	−0.0153	−0.1750	−0.0592	−0.0743	YES	YES	YES	YES
−	+	*	#	**7b**	HYD46	N(/N = C\c1ccc(Oc2ccc(cc2)c2nc3ccccc3s2)cc1)C(=O)c1ccc(cc1)[N+](=O)[O-]&	0.2527	0.2738	0.2289	0.3235	0.4476	−0.0211	0.0241	−0.0708	−0.1949	YES	YES	YES	YES
#	*	+	−	**7c**	HYD47	N(/N = C\c1ccc(Oc2ccc(cc2)c2nc3ccccc3s2)cc1)C(=O)c1ccc(Cl)cc1&	0.1123	0.2068	0.2806	0.2042	0.2379	−0.0945	−0.1683	−0.0922	−0.1256	YES	YES	YES	YES
*	#	−	+	**7d**	HYD48	N(/N = C\c1ccc(Oc2ccc(cc2)c2nc3ccccc3s2)cc1)C(=O)c1ccncc1&	0.0864	0.1383	0.1275	0.0722	0.0442	−0.0519	−0.0415	0.0138	0.0422	YES	YES	YES	No
+	−	#	*	**7e**	HYD49	N(/N = C\c1ccc(Oc2ccc(cc2)c2nc3ccccc3s2)cc1)C(=O)c1ccc(OC)cc1&	0.1320	0.1509	0.1373	0.1173	0.1308	−0.0189	−0.0053	0.0147	0.0012	YES	YES	YES	YES
−	+	*	#	**7f**	HYD50	N(/N = C\c1ccc(Oc2ccc(cc2)c2nc3ccccc3s2)cc1)C(=O)c1ccc(C)cc1&	0.3280	0.2096	0.2821	0.1669	0.1891	0.1184	0.0459	0.1611	0.1389	YES	YES	YES	YES
#	*	+	−	**7g**	HYD51	N(/N = C\c1ccc(Oc2ccc(cc2)c2nc3ccccc3s2)cc1)C(=O)c1ccc(Br)cc1&	0.2879	0.2068	0.2806	0.2042	0.2379	0.0811	0.0073	0.0838	0.0500	YES	YES	YES	YES
*	#	−	+	**7h**	HYD52	N(/N = C\c1ccc(Oc2ccc(cc2)c2nc3ccccc3s2)cc1)C(=O)c1cccnc1&	−0.0287	0.0927	0.1351	0.0723	0.0789	−0.1214	−0.1641	−0.1013	−0.1076	YES	YES	YES	YES
+	−	#	*	**7i**	HYD53	N(/N = C\c1ccc(Oc2ccc(cc2)c2nc3ccccc3s2)cc1)C(=O)c1ccco1&	−0.1026	−0.0257	−0.0230	0.0015	0.0640	−0.0769	−0.0800	−0.1045	−0.1666	YES	YES	YES	YES
−	+	*	#	**7j**	HYD54	N(/N = C\c1ccc(Oc2ccc(cc2)c2nc3ccccc3s2)cc1)C(=O)c1ccsc1&	−0.0160	−0.0732	0.0185	−0.1492	−0.0129	0.0572	−0.0345	0.1332	−0.0031	YES	YES	YES	YES
#	*	+	−	**7k**	HYD55	N(/N = C\c1ccc(Oc2ccc(cc2)c2nc3ccccc3s2)cc1)C(=O)c1cccc(C)c1&	−0.0255	0.0514	0.1521	0.0467	0.0599	−0.0769	−0.1776	−0.0727	−0.0854	YES	YES	YES	YES
*	#	−	+	**7l**	HYD56	N(/N = C\c1ccc(Oc2ccc(cc2OC)c2nc3ccccc3s2)cc1)C(=O)c1ccccc1&	0.1813	0.0749	0.2322	0.1470	0.1883	0.1064	−0.0512	0.0340	−0.0070	YES	YES	YES	YES
+	−	#	*	**7m**	HYD57	N(/N = C\c1ccc(Oc2ccc(cc2OC)c2nc3ccccc3s2)cc1)C(=O)c1ccc(cc1)[N+](=O)[O-]&	0.2082	0.2301	0.2046	0.2977	0.2519	−0.0219	0.0034	−0.0897	−0.0437	YES	YES	YES	YES
−	+	*	#	**7n**	HYD58	N(/N = C\c1ccc(Oc2ccc(cc2OC)c2nc3ccccc3s2)cc1)C(=O)c1ccc(Cl)cc1&	0.0447	0.1409	0.2127	0.1669	0.2264	−0.0962	−0.1677	−0.1222	−0.1817	YES	YES	YES	YES
#	*	+	−	**7o**	HYD59	N(/N = C\c1ccc(Oc2ccc(cc2OC)c2nc3ccccc3s2)cc1)C(=O)c1ccncc1&	−0.1157	0.0724	0.0597	0.0350	0.0327	−0.1881	−0.1754	−0.1510	−0.1484	YES	YES	YES	No
*	#	−	+	**7p**	HYD60	N(/N = C\c1ccc(Oc2ccc(cc2OC)c2nc3ccccc3s2)cc1)C(=O)c1ccc(OC)cc1&	0.1091	0.0452	0.0173	−0.0028	0.0085	0.0639	0.0917	0.1118	0.1006	YES	YES	YES	YES
+	−	#	*	**7q**	HYD61	N(/N = C\c1ccc(Oc2ccc(cc2OC)c2nc3ccccc3s2)cc1)C(=O)c1ccc(C)cc1&	0.3058	0.1437	0.2143	0.1297	0.1777	0.1621	0.0917	0.1763	0.1281	YES	YES	YES	YES
−	+	*	#	**7r**	HYD62	N(/N = C\c1ccc(Oc2ccc(cc2OC)c2nc3ccccc3s2)cc1)C(=O)c1ccc(Br)cc1&	0.1352	0.1409	0.2127	0.1669	0.2264	−0.0057	−0.0777	−0.0317	−0.0912	YES	YES	YES	YES
#	*	+	−	**7s**	HYD63	N(/N = C\c1ccc(Oc2ccc(cc2OC)c2nc3ccccc3s2)cc1)C(=O)c1cccnc1&	0.2844	0.0269	0.0673	0.0351	0.0674	0.2575	0.2171	0.2489	0.2170	YES	YES	YES	YES
*	#	−	+	**7t**	HYD64	N(/N = C\c1ccc(Oc2ccc(cc2OC)c2nc3ccccc3s2)cc1)C(=O)c1ccco1&	0.0255	−0.0915	−0.0909	−0.0357	0.0525	0.1170	0.1169	0.0617	−0.0270	YES	YES	YES	YES
+	−	#	*	**7u**	HYD65	N(/N = C\c1ccc(Oc2ccc(cc2OC)c2nc3ccccc3s2)cc1)C(=O)c1ccsc1&	−0.1352	−0.1391	−0.0493	−0.1864	−0.0243	0.0039	−0.0857	0.0514	−0.1109	YES	YES	YES	YES
−	+	*	#	**7v**	HYD66	N(/N = C\c1ccc(Oc2ccc(cc2OC)c2nc3ccccc3s2)cc1)C(=O)c1cccc(C)c1&	0.1060	−0.0144	0.0842	0.0095	0.0484	0.1204	0.0218	0.0965	0.0576	YES	YES	YES	YES

[a]Experimental $pPI_{\alpha-amylase}$ was calculated from the percentage inhibition given in Table 2 using Equation (1).

Table 4. The detailed description of SMILES attributes.

S. no.	SMILES notation	Comments
1	S_k	SMILES-atoms, that is, one or two symbols which cannot be examined separately
2	SS_k	A combination of two SMILES atoms
3	SSS_k	A combination of three SMILES atoms
4	BOND	The presence or absence of double ('='), triple ('#') and stereochemical ('@') bonds
5	HALO	Presence or absence of halogens
6	NOSP	Presence or absence of nitrogen, oxygen, sulfur and phosphorus
7	PAIR	The simultaneous presence of two SMILES atoms from the BOND, NOSP and HALO
8	C_{max}	Total number of rings (the range 0 … 9)
9	N_{max}	Total number of nitrogen atoms in the molecular structure
10.	O_{max}	Total number of oxygen atoms in the molecular structures
11.	S_{max}	Total number of sulphur atoms in the molecular structure

considered as leading models. The mathematical representation of leading QSAR model developed by CORAL software using target function **TF$_1$** (without IIC) and **TF$_2$** (with IIC) are given below:

$$pPI_{\alpha\text{–amylase}} = -10.9652922\ (\pm\ 0.3110474) + 0.2760362\ (\pm\ 0.0076075) * DCW(6,7)$$ using **TF**1

$n = 17$, $R^2 = 0.8392$, CCC = 0.9126, IIC = 0.8143, $Q^2 = 0.7981$ (training); $n = 17$, $R^2 = 0.8357$, CCC = 0.8952, IIC = 0.6095, $Q^2 = 0.7931$ (invisible training); $n = 16$, $R^2 = 0.7879$, CCC = 0.8749, IIC = 0.8123, $Q^2 = 0.7244$ (calibration); $n = 16$, $R^2 = 0.7548$, CCC = 0.8668, IIC = 0.6516, $Q^2 = 0.6921$ (validation).

$$pPI_{\alpha\text{–amylase}} = -7.6186542\ (\pm\ 0.1453246) + 0.1407535\ (\pm\ 0.0025541) * DCW(5,13)$$ using **TF**2

$n = 17$, $R^2 = 0.8746$, CCC = 0.9331, IIC = 0.6547, $Q^2 = 0.8491$ (training); $n = 17$, $R^2 = 0.8317$, CCC = 0.8976, IIC = 0.4154, $Q^2 = 0.7866$ (Invisible training); $n = 16$, $R^2 = 0.7890$, CCC = 0.8812, IIC = 0.8882, $Q^2 = 0.7072$ (calibration); $n = 16$, $R^2 = 0.8587$, CCC = 0.9237, IIC = 0.8932, $Q^2 = 0.8091$ (validation).

As we can see from the above and other QSAR models given in Table 5, the standard error of coefficients of DCWs and constant parameters is very low and each of these modelled QSAR equations can be applied to predict $pPI_{\alpha\text{–amylase}}$. The numerical data of experimental $pPI_{\alpha\text{–amylase}}$, predicted $pPI_{\alpha\text{–amylase}}$, their difference and applicability domain (AD) of newly synthesized compounds are given in Table 3 (see Supplementary Information also). It can be seen that the calculated $pPI_{\alpha\text{–amylase}}$ at different concentrations for the dataset were in good correlation with its experimental $pPI_{\alpha\text{–amylase}}$ values from QSAR models calculated with **TF$_1$** and **TF$_2$** which are presented in Figure 4. The robustness and predictability of developed QSAR models had been ascertained by the various statistical parameters such as R^2, CCC, Q^2F_1, Q^2F_2, Q^2F_3, Q^2, $C_{R_p^2}$ and metric R_m^2 (Table 5). The robustness of QSAR models was also quantified by the *Y*-randomization test (Table 5) (for details see Supplementary Information). For the *Y*-randomization test, the constructed models were free from chance correlation if the value of $C_{R_p^2}$ was more than 0.5 (Ojha & Roy, 2011).

The IIC was applied as a final statistical parameter to authenticate the build QSAR models. The role of IIC in developing a robust and reliable QSAR model was well cited in the literature (Kumar et al., 2019c; Manisha et al., 2019; Nimbhal et al., 2020; Toropova & Toropov, 2019c). Therefore, QSAR models build by **TF$_2$** using IIC are more robust and reliable than by **TF$_1$**. In the Monte-Carlo optimization, the ideal model was chosen on the basis of the higher coefficient of determination (R^2) for validation set and higher IIC for the calibration set. The QSAR model was rated right or wrong according to the method given in the literature (Kumar & Kumar, 2020; Manisha et al., 2019; Nimbhal et al., 2020; Toropova & Toropov, 2019b). After fastidious assessment of statistical outcomes depicted in Table 5 the right and wrong rating was given to each statistical parameter.

All statistical parameters excluding Q^2 and MAE showed a better model for splits 1 correctly. Similarly, in the case of split 2, only two parameters Q^2 and ΔR_m^2 predicted model wrongly. For split 3, all statistical criteria apart from *Y*-test exhibited better models correctly. For split 4, only four criterion Q^2, *F*, MAE, ΔR_m^2 showed a better model wrongly. All models were correctly predicted by the IIC.

The AD is a significant parameter of OECD principles and those compound which falls outside the AD are defined as outliers. In the case of combined dataset, no outlier was found for the developed QSAR models using **TF$_1$** and **TF$_2$**. It has been observed that hydrazones of 4-pyridylcarbaldehyde (**7d** and **7o**) at different concentrations (HYD04, HYD15, HYD26, HYD37, HYD48 and HYD59) and compound **7s** at 25 μg/mL (HYD41) of split 4 only was outside the AD for the developed QSAR models using **TF$_2$**. On the other hand, no outlier was found for split 1 and split 4 using **TF$_1$**, but compounds **7b** (HYD02, HYD24, HYD46) and **7m** (HYD13, HYD35, HYD57) of split 2 at each concentration and were outside the AD for the developed QSAR models. In split 3, compounds **7b** (HYD24)**, 7i** (HYD31)**, 7t** (HYD42) at 25 μg/mL and **7m** (HYD13, HYD35, HYD57) all concentrations were found outlier.

4. Interpretation of structure–activity relationship by mechanistic interpretation

A mechanistic interpretation means that structural features responsible for the increase and decrease of an endpoint can be obtained from the constructed QSAR models. In Monte Carlo optimization method, the SMILES structural attributes (SAk) had been interpreted for investigating the molecular information, which was involved in α-amylase inhibition study through the analysis of the correlation weight, the

Table 5. The statistical parameter of QSAR models for hydrazone set using $\mathbf{TF_1}$ and $\mathbf{TF_2}$.

Split	Target Function	SET	*N*	R^2	CCC	IIC	Q^2	Q^2F_1	Q^2F_2	Q^2F_3	*S*	MAE	*F*	Avg Rm^2	ΔRm^2	*Y*-test	$CR_p{}^2$	Equation
1	TF_1	Training	17	0.8392	0.9126	0.8143	0.7981				0.098	0.081	78			0.0273	0.8254	$pPI_{\alpha\text{-amylase}} = -10.9652922$
		InvTrain	17	0.8357	0.8952	0.6095	0.7931				0.109	0.086	76			0.0669	0.8016	(±0.3110474) + 0.2760362 (±0.0076075) * DCW(6,7)
		Calib	16	0.7879	0.8749	0.8123	**0.7244**	0.7854	0.7853	0.7668	0.120	**0.089**	52	0.6952	0.1546	0.1291	0.7205	
		Valid	16	0.7548	0.8668	0.6516	0.6921				0.109	0.089	43	0.6724	0.0181	0.0561	0.7262	
	TF_2	Training	17	0.8746	0.9331	0.6547	0.8491				0.086	0.063	105			0.0895	0.8287	$pPI_{\alpha\text{-amylase}} = -7.6186542$
		InvTrain	17	0.8317	0.8976	0.4154	0.7866				0.109	0.086	74			0.0685	0.7968	(±0.1453246) + 0.1407535 (±0.0025541)
		Calib	16	0.7890	**0.8812**	**0.8882**	0.7072	**0.7890**	**0.7890**	**0.7710**	**0.118**	0.098	**52**	**0.7087**	**0.1513**	**0.0845**	**0.7455**	* DCW(5,13)
		Valid	16	**0.8587**	0.9237	0.8932	0.8091				0.084	0.068	85	0.8064	0.0460	0.0687	0.8236	
	Comments			Correct	Correct	Correct	Wrong	Correct	Correct	Correct	Correct	Wrong	Correct	Correct	Correct	Correct	Correct	
2	**TF_1**	Training	17	0.8801	0.9362	0.8338	0.8374				0.086	0.066	110			0.0388	0.8605	$pPI_{\alpha\text{-amylase}} = -7.2513374$
		InvTrain	17	0.9082	0.9350	0.7787	0.8874				0.087	0.076	148			0.0579	0.8788	(±0.2388291) + 0.2125887 (±0.0066788) * DCW(2,8)
		Calib	16	0.8640	0.9182	0.6911	**0.8243**	0.8286	0.8221	0.8737	0.088	0.076	89	0.8132	**0.0302**	0.0695	0.8285	
		Valid	16	0.7677	0.8697	0.6476	0.6860				0.125	0.101	46	0.6781	0.1650	0.0832	0.7249	
	TF_2	Training	17	0.8413	0.9138	0.8153	0.7987				0.099	0.078	80			0.0471	0.8174	$pPI_{\alpha\text{-amylase}} = -11.8804062$
		InvTrain	17	0.7975	0.8834	0.8252	0.7445				0.115	0.096	59			0.0167	0.7890	(±0.3466972) + 0.2579762 (±0.0073653)
		Calib	16	0.8704	**0.9260**	**0.9329**	0.8200	**0.8526**	**0.8470**	**0.8914**	**0.082**	**0.065**	**94**	**0.8208**	0.0760	**0.0318**	**0.8543**	* DCW(6,13)
		Valid	16	**0.7937**	0.8741	0.6618	0.7162				0.121	0.099	54	0.6406	0.1693	0.0682	0.7588	
	Comments			Correct	Correct	Correct	Wrong	Correct	Correct	Correct	Correct	Correct	Correct	Correct	Wrong	Correct	Correct	
3	**TF_1**	Training	16	0.9146	0.9554	0.5739	0.8830				0.075	0.050	150			0.0385	0.8951	$pPI_{\alpha\text{-amylase}} = -21.6553652$
		InvTrain	16	0.9157	0.9447	0.9508	0.8920				0.076	0.064	152			0.0279	0.9016	(±0.5922651) + 0.3351006 (±0.0089669) * DCW(1,7)
		Calib	17	0.7454	0.8590	0.6582	0.6791	0.6967	0.6967	0.6742	0.134	0.109	44	0.6634	0.0151	**0.0623**	0.7135	
		Valid	17	0.7202	0.8450	0.7247	0.6513				0.146	0.126	39	0.6297	0.0978	0.0663	0.6862	
	TF_2	Training	16	0.8353	0.9103	0.7109	0.7735				0.105	0.084	71			0.0348	0.8178	$pPI_{\alpha\text{-amylase}} = -8.2153672$
		InvTrain	16	0.8955	0.9435	0.6656	0.8642				0.073	0.061	120			0.0498	0.8702	(±0.3411089) + 0.1623760 (± 0.0064083)
		Calib	17	0.8311	**0.9104**	**0.9115**	**0.7903**	**0.8290**	**0.8290**	**0.8163**	**0.101**	**0.079**	**74**	**0.7713**	**0.0448**	0.1079	**0.7753**	* DCW(5,17)
		Valid	17	**0.7806**	0.8721	0.6223	0.7218				0.123	0.104	53			0.0444	0.7581	
	Comments			Correct	Correct	Correct	Correct	Correct	Correct	Correct	Correct	Correct	Correct	Correct	Correct	Wrong	Correct	
4	**TF_1**	Training	16	0.8009	0.8895	0.6960	0.7374				0.093	0.074	56			0.0847	0.7574	$pPI_{\alpha\text{-amylase}} = -7.0936234$ (±
		InvTrain	16	0.7956	0.8337	0.7531	0.7283				0.128	0.108	54			0.0868	0.7509	0.2980071) + 0.1336658 (±0.0053357) * DCW(5,5)
		Calib	17	0.7501	0.8076	0.8433	**0.6892**	0.7060	0.6977	0.6593	0.137	**0.106**	**45**	0.6389	0.1852	0.0617	0.7186	
		Valid	17	0.7533	0.8438	0.5734	0.7013				0.123	0.096	46	0.6404	0.1797	0.0346	0.7358	
	TF_2	Training	16	0.9051	0.9502	0.7400	0.8736				0.064	0.046	134			0.0777	0.8654	$pPI_{\alpha\text{-amylase}} = -7.3740792$
		InvTrain	16	0.8570	0.8992	0.7907	0.8062				0.105	0.083	84			0.0341	0.8398	(±0.2017983) + 0.1567343 (±0.0041021)
		Calib	17	0.7410	**0.8488**	**0.8608**	0.6795	**0.7417**	**0.7345**	**0.7005**	**0.128**	0.111	43	**0.6528**	**0.1070**	**0.0149**	**0.7336**	* DCW(3,16)
		Valid	17	**0.8076**	0.8715	0.7644	0.7537				0.111	0.088	63	0.6724	0.1555	0.0491	0.7827	
	Comments			Correct	Correct	Correct	Wrong	Correct	Correct	Correct	Correct	Wrong	Wrong	Correct	Wrong	Correct	Correct	

Bold signifies the best prediction for calibration and validation set.

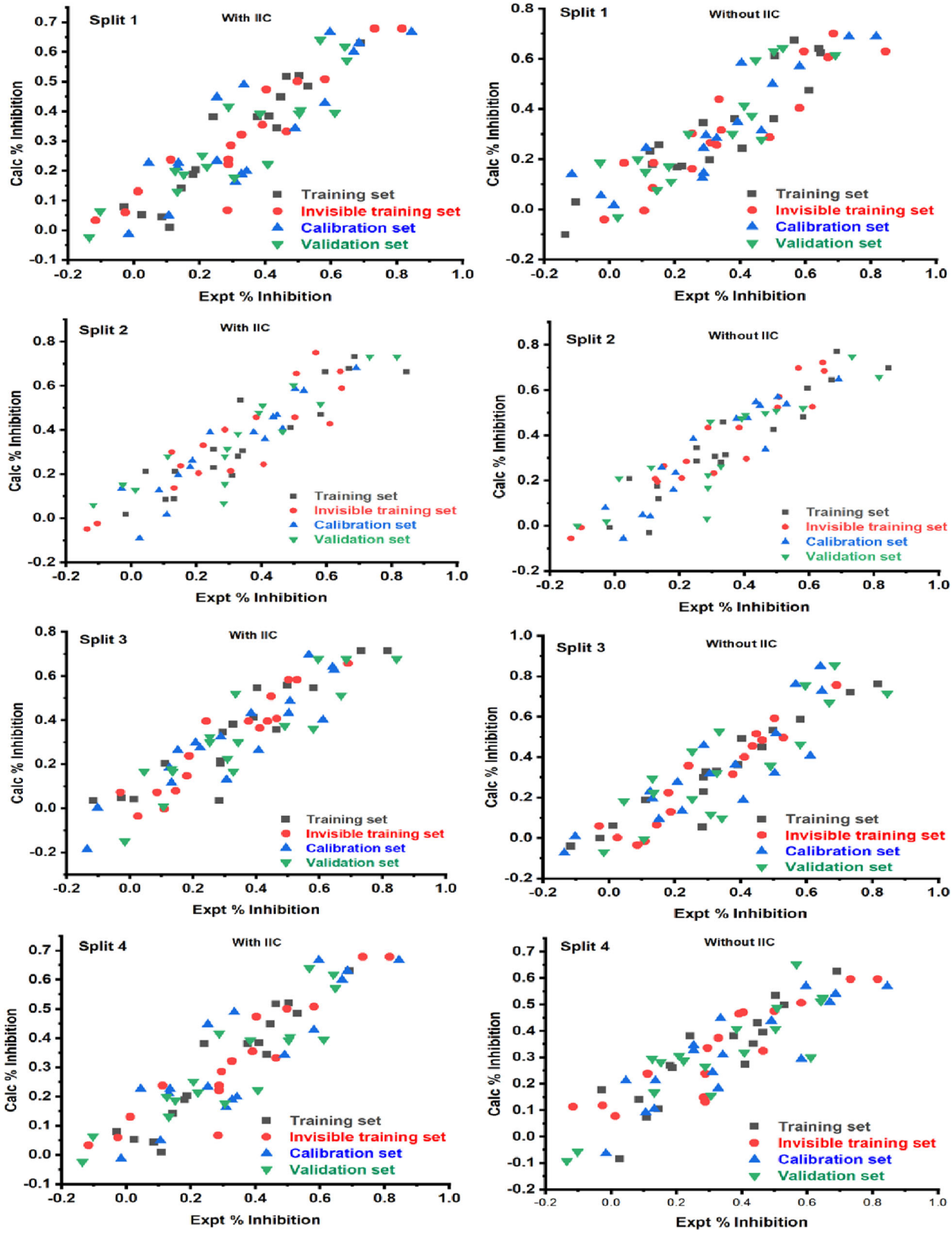

Figure 4. Plots of observed *versus* calculated $pPI_{\alpha-amylase}$ values for all splits with both TF_1 and TF_2.

optimal descriptor, obtained from QSAR modelling. The promoters of increase and decrease of the α-amylase inhibition were extracted from these structural attributes (SAk).

This was done by splitting the data samples into the following four classes: (i) List of promoters of $pPI_{\alpha-amylase}$ increase (if all correlation weights are positive in three independent Monte Carlo optimization runs) ; (ii) List of promoters of pIC_{50} decrease (all correlation weights are negative in three independent Monte Carlo optimization runs); (iii) Attributes with an unclear role (the correlation weights have

Table 6. Promoter of endpoint increase and endpoint decrease for hydrazones.

No.	SAk	Remarks	CWs Probe 1	CWs Probe 2	CWs Probe 3	NSs	NSc	NSv	Defect [SAk]
		Promoter of endpoint increase							
1	(… … …..	Branching	0.1264	0.0946	0.0862	17	17	16	0.0000
2	++++N—O===	Presence of nitrogen with oxygen	0.2795	0.3311	0.3342	17	17	16	0.0000
3	++++N—S===	Presence of nitrogen with sulphur	0.4449	0.8671	0.6048	17	17	16	0.0000
4	++++O—B2==	Presence of oxygen with double bond	0.5658	0.4520	0.5057	17	17	16	0.0000
5	++++O—S===	Presence of oxygen with sulphur	0.4642	0.2960	0.7436	17	17	16	0.0000
6	++++S—B2==	Presence of sulfur with double bond	0.3831	0.2395	0.5982	17	17	16	0.0000
7	/…(… ….	Trans bond with branching	0.0836	0.7018	0.2115	17	17	16	0.0000
8	/… … …..	Trans bond	0.4370	0.5959	0.9931	17	17	16	0.0000
9	1…(… ….	One aromatic ring with branching	0.2313	0.2336	0.5732	17	17	16	0.0000
10	1… … …..	One aromatic ring	0.4043	0.6466	0.1439	17	17	16	0.0000
11	2…(… ….	Two aromatic ring with branching	0.0604	0.3143	0.4558	17	17	16	0.0000
12	2… … …..	Two aromatic ring	0.4832	0.9737	0.9681	17	17	16	0.0000
13	2…c…(…	2nd ring having aromatic carbon with branching	0.2169	0.3386	0.2986	17	17	16	0.0000
14	=…N…/…	Combination of double bond, nitrogen and trans bond	0.3663	0.5074	0.4671	17	17	16	0.0000
15	=…O…(…	Combination of double bond, oxygen and branching	0.0284	0.1701	0.1755	17	17	16	0.0000
16	C…(…1…	Aliphatic carbon with branching on first ring	0.6403	0.2959	0.4749	17	17	16	0.0000
17	C…=… ….	Aliphatic carbon with double bond	0.1445	0.5515	0.3337	17	17	16	0.0000
18	BOND10000000	Presence of double bond	0.7416	0.9098	1.0135	17	17	16	0.0000
		Promoter of endpoint decrease							
1	(…C…(…	Branching on both side of aliphatic carbon	−0.0921	−0.2289	−0.0813	17	17	16	0.0000
2	1…c…(…	Combination one ring, aromatic carbon and branching	−0.2164	−0.3896	−0.3913	17	17	16	0.0000
3	c…(… ….	aromatic carbon with branching	−0.1215	−0.0034	−0.1775	17	17	16	0.0000
4	c…1… ….	aromatic carbon with one aromatic ring	−0.2709	−0.2359	−0.1524	17	17	16	0.0000
5	&… … …..	Activity performed at 25 mg/mL	−0.5493	−0.4821	−0.1239	6	6	5	0.0037
6	1…&… ….	Activity performed at 25 mg/mL for a compound having one aromatic ring	−0.1856	−0.5110	−0.0030	5	5	5	0.0018

both negative and positive value in three independent Monte Carlo optimization runs) and (iv) Blocked (rare) attributes (not involved in three independent Monte Carlo optimization runs). Lists of the most significant promoters of $pPI_{\alpha-amylase}$ are presented in Table 6.

The common structural attributes (SAk) for increasing the endpoint $pPI_{\alpha-amylase}$ in split 1 are: (i) the presence of nitrogen with oxygen; (ii) the presence of nitrogen with sulfur; (iii) the presence of oxygen with sulfur; (iv) one aromatic ring with branching; (v) aromatic ring surrounded by two sp^2 hybridized carbon. The common SAk for a promoter of decreasing the endpoint is the inhibition study performed at 12.5 µg/mL concentration. The inhibitory potential of compound **7k** (*o*-methyl group) was less than the **7a** (Table 2). The decrease in the activity of compound **7k** was due to the presence of an *ortho*-methyl group and was confirmed by putting the above SMILES together to generate a sequence …c(C)c1 of SMILES.

5. Molecular docking studies

Recently, the computer-assisted drug design (CADD) has been accepted as a successful methodology of drug design & discovery to understand the structural design of a drug candidate. It is quite fast, cost-effective and result-oriented fruitful *in silico* technique (Ferreira et al., 2015; Macalino et al., 2015). The active site of a target protein can be assessed using molecular docking to explore the probable binding modes of a drug. The molecular docking studies were performed with Auto Dock Vina software to predict the probable mode of binding for most potent compounds **7n**. Docking simulation of **7n** was performed with the active site of *Aspergillus oryzae* α-amylase (**PDB ID: 7TAA**) to establish the binding conformation and interactions responsible for their activity. The most active compounds **7n** were sketched using ChemAxon software and these were changed into 3D structures using the MMFF94 force field.

5.1. Docking analysis of α-amylase

Binding pose with the highest binding affinity for docked conformation of **7n** is shown in Figure 5. The ligand fits snugly in the active site of the protein. It has been revealed from Figure 5 that various interactions in terms of hydrogen bonding, hydrophobic and electrostatic interactions are mainly responsible for anchoring of the compound **7n** in the active site of α-amylase. The main hydrophobic interaction are observed with Leu^{173}, Tyr^{82}, Leu^{166}, Leu^{232}, Tyr^{155}, Trp^{83}, Tyr^{75}. The phenyl ring of ether linkage and the phenyl group of carbonyl group are involved in π–π interactions with residues Hie^{80}, Arg^{344}, Trp^{83} and Tyr^{75}. The NH of hydrazone is involved in H-bond with Gln^{35}. All other interactions observed in the protein-ligand complex of 7TAA:**7n** are shown in Figure 5. In case of α-amylase, Glu^{230} and Asp^{206} are the residues responsible for the catalytic activity in hydrolytic reactions (Svensson, 1994). From the docking studies, it has been revealed that presence of interactions between **7n** and (Tyr^{82}, Arg^{204} and Glu^{230}) of α-amylase are similar to those responsible for α-amylase inhibition by acarbose as shown in Figure 5.

6. Molecular dynamics

Molecular dynamics simulation was performed with the docked conformation of **7n** with high binding affinity and low binding energy for 100 ns to analyse the stability of protein–ligand complex in physiological condition. Both RMSD (Å) and RMSF (Å) values were analysed for the protein–ligand

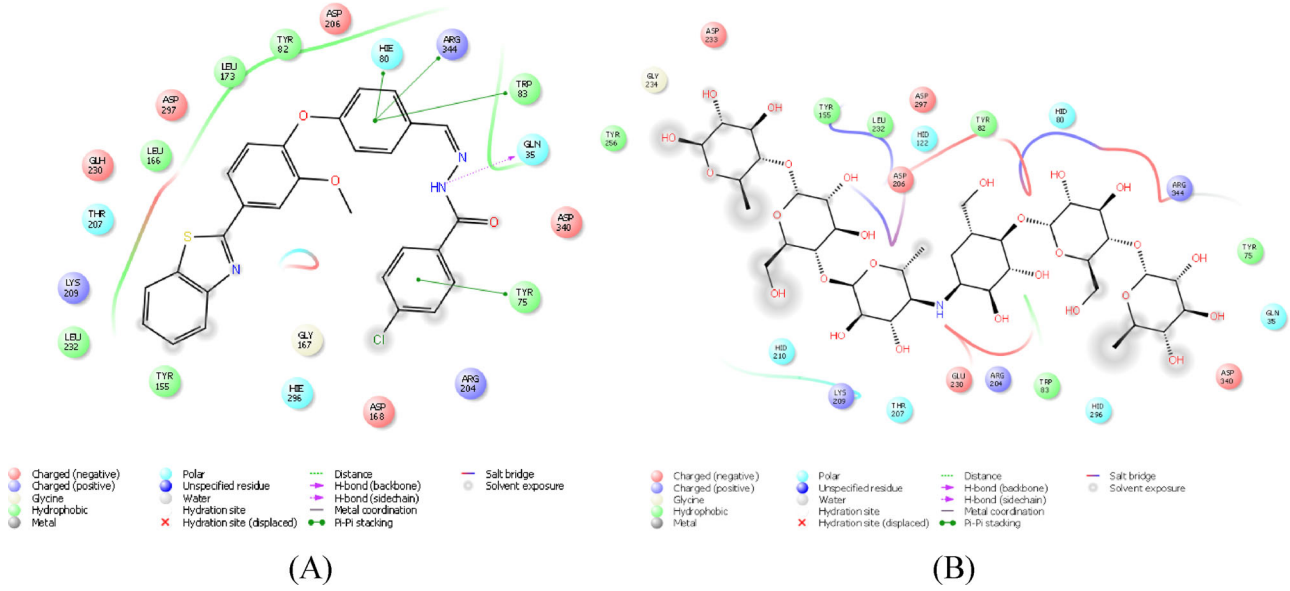

Figure 5. Interactions (dashed lines) of compounds with active site residues of ***Aspergillus oryzae*** α-amylase (a) **7n**; and (b) **Acarbose**.

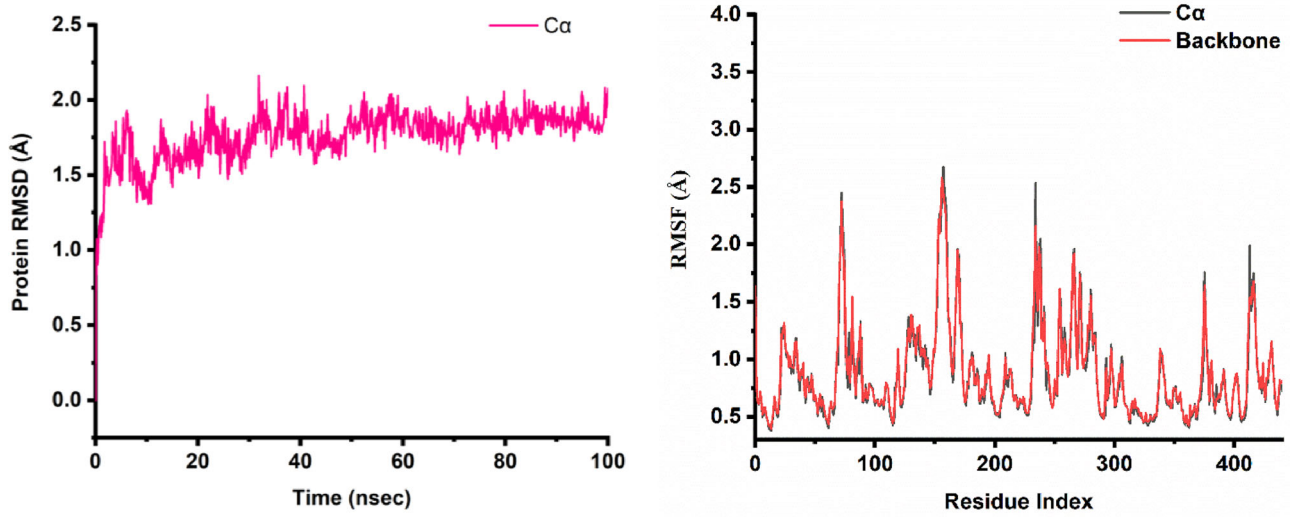

Figure 6. RMSD (Å) and RMSF (Å) of simulated protein **7TAA.*pdb*** with **7n**.

complex. The stability of the protein depends upon RMSD, protein with lower RMSD in dynamic simulations exhibits greater stability. The RMSD of free protein get stabilised after 20 ns and remained below 2 Å for the remaining simulation (Figure 6). Moreover, the deviation observed in RMSF during simulation for each amino acid residue with respect to Cα carbon atom was insignificant. The flexibility of residue on ligand binding was analysed using metrics of root mean square fluctuations (RMSFs), highest flexibility was observed with RMSF of Thr^{72} (Cα:2.53 Å; backbone:2.37 Å), Asp^{157} (Cα: 2.67 Å; backbone: 2.42 Å), Glu^{156} (Cα: 2.50 Å; backbone: 2.58 Å) and Gly^{234} (Cα: 2.53 Å; backbone: 2.16 Å), however lower RMSF was observed for Phe^{13} (Cα: 0.37 Å; backbone: 0.39 Å), Tyr^{12} (Cα: 0.39 Å; backbone: 0.43 Å) and Trp^{61} (Cα: 0.40 Å; backbone: 0.43 Å) (Figure 6).

The protein–ligand complex shows significant interactions with different amino acids, from Gln^{35} to Leu^{69}, Gln^{71} to Tyr^{82}, Trp^{83} to Asn^{121}, His^{122} to Glu^{156}, Gln^{158} to Thr^{170}, Val^{171} to Lys^{209} and His^{210} to Arg^{340}. The ligand is stabilised by majority of hydrophobic interactions with 5%–70% of simulation time with residues Tyr^{75}, Trp^{83}, Ile^{152}, Tyr^{155}, Leu^{166}, Val^{171} and Leu^{173} (Figure 7). The 2D interaction diagram reveals various hydrophobic and hydrogen bonding interactions present in this protein–ligand complex. The NH group of hydrazone donated one hydrogen bond to Asp^{168} with 13%, the carbonyl group of hydrazide accepted one hydrogen bond from Gln^{71} with 11% of simulation time. The π–π stacking of Trp^{83} and Tyr^{75} with phenyl ring of hydrazide is 31% and 12%, respectively (Figure 7).

7. Conclusion

In this study, 22 novel (*E*)-*N*′-(4-(4-(benzo[*d*]thiazol-2-yl)aryloxy)benzylidene)-(aryl)hydrazide (**7a–7v**) compounds were synthesized. The synthesis of compounds **7a–7v** can be achieved by the condensation reaction of 4-(4-

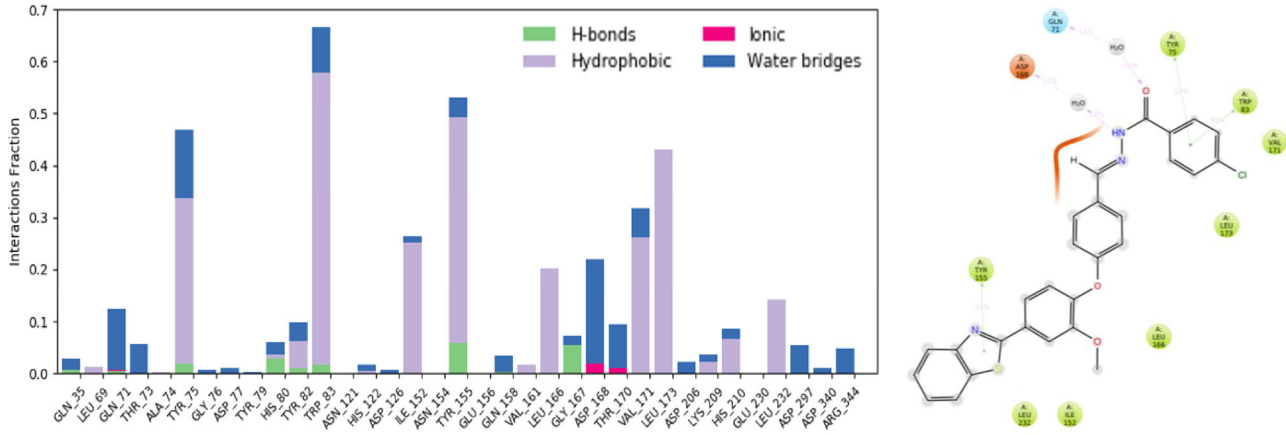

Figure 7. Interaction fraction and 2D interaction diagram of **7TAA** complexed with **7n**.

(benzo[*d*]thiazol-2-yl)aryloxy)benzaldehyde (**5a–5b**) with corresponding aryl/heteroaryl hydrazide (**6a–6k**) in refluxing EtOH:THF (80:20, v/v) in the presence of the catalytic amount of acetic acid. All the newly synthesized compounds and the standard drug, that is, acarbose were subjected to *in vitro* α-amylase inhibition activity at three different concentrations (50 μg/mL, 25 μg/mL and 12.5 μg/mL). Among these, compound **7n** at 50 μg/mL concentration showed a remarkable α-amylase inhibition, that is, 87.5% when compared with standard acarbose (77.96%, 71.17% and 67.24% at 50 μg/mL, 25 μg/mL and 12.5 μg/mL concentration), respectively. The percentage inhibition at various concentration was also predicted by developing the robust QSAR models using the balance of correlation method in CORAL software. The chemical structures at different concentration with optimal descriptors were represented by SMILES. A data set of 66 SMILES of 22 hydrazones at three distinct concentrations were prepared. The significance of the IIC with AD was also studied at depth. A QSAR models with best $R^2_{validation} = 0.8587$ for split 1 was considered as a leading model. The outliers and promoters of increase and decrease of endpoint were also extracted independently from the leading model. Docking studies of compounds **7n** were performed against the active site of *A. oryzae* α-amylase (**PDB ID: 7TAA**). The docking studies revealed that the binding interactions found between **7n** and α-amylase are similar to those responsible observed in case of acarbose. MD simulations performed on protein–ligand complex for 100 ns have strengthened the findings of docking studies. The RMSD of free protein get stabilised after 20 ns and remained below 2 Å for the remaining simulation. Moreover, the deviation observed in RMSF during simulation for each amino acid residue with respect to Cα carbon atom is insignificant.

8. Experimental

Structures of all the compounds were identified by their spectral data. Silica gel (60 F_{254}) plates (precoated aluminium plates) from Merck were used to monitor the reaction progress. All the melting points were determined in open glass capillary tubes and are uncorrected. In IR absorption spectra, the values are expressed as ν_{max} cm^{-1} and were obtained using Perkin Elmer FTIR spectrophotometer and Cary 660 Agilent IR spectrophotometer. The ^1H NMR and ^{13}C NMR spectra were recorded on Bruker (Avance-II) at 400 MHz & 500 MHz in DMSO-d_6 using tetramethylsilane (TMS) as an internal standard. Chemical shifts (δ) and coupling constants (J) are expressed in ppm and Hz, respectively. HRMS analysis was performed using LC–MS on SCIEX 5600$^+$QTOF operating at positive scan mode (120,000 FWMH) in a range of 100–1000 *m/z*. All chemicals used were supplied by Sigma-Aldrich, Avra and Merck chemical companies.

Synthesis of 2-arylbenzothiazole (3a–3b)

To a mixture of 2-aminothiophenol **1** (1.0 mmol) and *p*-hydroxybenzaldehyde (**2a**) (1.0 mmol) or vanillin (**2b**) (1.0 mmol) in a vial, added SiO_2–HNO_3 (2 wt% of the aldehyde) and the contents were shaken at room temperature (Kumar et al., 2015) (Scheme 1). An instant exothermic reaction occurred with the completion of the reaction (as monitored on TLC) and reaction mixture became yellowish-orange solid that was directly chromatographed over silica gel column using petroleum ether:ethyl acetate (80:20, v/v) with the increasing proportion of ethyl acetate to afford pure 2-arylbenzothiazole (**3a**–**3b**).

Synthesis of 4-(4-(benzo[d]thiazol-2-yl)aryloxy) benzaldehyde (5a–5b)

A mixture of 2-arylbenzothiazole (**3a–3b**) (1.0 mmol), potassium carbonate (K_2CO_3) (1.2 mmol) in DMSO (10 mL) and 4-fluorobenzaldehyde (**4**) (1.1 mmol) was taken in a round bottom flask (50 mL) and heated at 120 °C for 4–5 h on an oil bath. After completion of the reaction as monitored by TLC using petroleum ether:ethylacetate (80:20, v/v), the reaction was quenched using ice and the solid, so formed, was filtered under suction and recrystallized from ethanol to get the desired product (**5a–5b**).

4-(4-(Benzo[d]thiazol-2-yl)phenoxy)benzaldehyde (5a)

Yield: 87%; **M.pt:** 118–120 °C; **IR (ν_{max} cm^{-1}, KBr):** 3061, 2732, 1702, 1593; **^1H NMR (400 MHz, δ (ppm) DMSO-d_6):**

9.98 (s, 1H, C**H**O), 8.20–8.14 (m, 3H, $H_{19}/H_{21,}$ H_5), 8.07 (dd, $J = 7.9$ Hz, 1.1 Hz, 1H, H_8), 7.99 (d, $J = 8.8$ Hz, 2H, H_{11}/H_{15}), 7.58–7.54 (m, 1H, H_7), 7.49–7.45 (m, 1H, H_6), 7.31 (d, $J = 8.8$ Hz, 2H, H_{18}/H_{22}), 7.28 (d, $J = 8.8$ Hz, 2H, H_{12}/H_{14}); **^{13}C NMR (100 MHz, δ (ppm) DMSO-d_6):** 191.59, 166.35, 161.17, 157.65, 153.57, 134.47, 132.06, 131.99, 129.41, 129.16, 126.66, 125.47, 122.79, 122.34, 120.26, 118.66; **Anal. Calc. For $C_{20}H_{13}NO_2S$:** C, 72.49; H, 3.95; N, 4.23. **Found:** C, 72.44; H, 3.91; N, 4.19.

4-(4-(Benzo[d]thiazol-2-yl)-2-methoxyphenoxy)benzaldehyde (5b)

Yield: 89%; **M.pt:** 123-125 °C; **IR (ν_{max} cm^{-1}, KBr):** 1685, 1580, 1500, 1482, 1275; **^{1}H NMR (400 MHz, δ (ppm) DMSO-d_6):** 9.92 (s, 1H, –C**H**O), 8.16 (d, $J = 7.72$ Hz, 1H, H_5), 8.10 (d, $J = 7.96$ Hz, 1H, H_8), 7.93–7.88 (m, 3H, $H_{19}/H_{21,}$ H_{15}), 7.72 (dd, $J = 8.24$, 2.04 Hz, 1H, H_{11}), 7.59–7.55 (m, 1H, H_7), 7.51–7.47 (m, 1H, H_6), 7.36 (d, $J = 8.12$ Hz, 1H, H_{12}), 7.10 (d, $J = 8.74$, 2H, H_{18}/H_{22}), 3.89 (s, 3H, –OCH_3); **^{13}C NMR (100 MHz, δ (ppm) DMSO-d_6):** 191.45, 166.445, 162.19, 153.46, 151.73, 144.68, 134.59, 131.92, 131.12, 131.06, 126.73, 125.60, 122.99, 122.87, 122.36, 120.87, 116.23, 111.20, 55.95; **Anal. Calc. For $C_{21}H_{15}NO_3S$:** C, 69.79; H, 4.18; N, 3.88. **Found:** C, 69.75; H, 4.17; N, 3.85.

Synthesis of N′-(4-(4-(benzo[d]thiazol-2-yl)aryloxy) benzylidene)-(aryl)hydrazide (7a–7v)

To the stirred solution of 4-(4-(benzo[*d*]thiazol-2-yl)aryloxy)-benzaldehyde (**7a**–**7b**) (1.0 mmol) in EtOH:THF (4:1; 20 mL), aryl/heteroaryl hydrazide (**6a**–**6k**) (1.0 mmol) was added in the presence of a catalytic amount of acetic acid and the solution was refluxed for 6 h. The extent of the reaction was examined by TLC using petroleum ether:ethyl acetate (80:20, v/v). On completion of the reaction, the mixture was allowed to cool at room temperature and the solid thus obtained was filtered and recrystallized from absolute ethanol to afford *N′*-(4-(4-(benzo[*d*]thiazol-2-yl)aryloxy)benzylidene)-(aryl)hydrazides (**7a–7v**) in good to excellent yield.

(E)-N′-(4-(4-(benzo[d]thiazol-2-yl)phenoxy)benzylidene) benzohydrazide (7a)

Yield: 84%; **M.pt:** 246–248 °C; **IR (ν_{max} cm^{-1}, KBr):** 3214, 3055, 1638, 1478, 1250; **^{1}H NMR (400 MHz, δ (ppm) DMSO-d_6):** 11.89 (s, 1H, NH), 8.49 (s, 1H, H_{23}), 8.17–8.15 (m, 3H, H_{11}/H_{15}, H_5), 8.06 (d, $J = 7.92$ Hz, 1H, H_8), 7.93 (d, $J = 7.2$ Hz, 2H, H_{28}/H_{32}), 7.83 (d, $J = 8.7$ Hz, 2H, H_{19}/H_{21}), 7.63–7.53 (m, 4H, H_7, H_{29}/H_{31}, H_{30}), 7.49–7.45 (m, 1H, H_6), 7.26–7.21 (m, 4H, H_{18}/H_{22}, H_{12}/H_{14}); **^{13}C NMR (100 MHz, δ (ppm) DMSO-d_6):** 166.49, 158.84, 157.19, 153.56, 146.94, 142.64, 135.88, 134.39, 133.37, 131.74, 130.33, 129.31, 129.11, 128.47, 127.57, 126.65, 125.41, 122.70, 122.33, 119.49, 119.22; **Anal. Calc. For $C_{27}H_{19}N_3O_2S$:** C, 72.14; H, 4.26; N, 9.35. **Found:** C, 72.09; H, 4.21; N, 9.29.

(E)-N′-(4-(4-(benzo[d]thiazol-2-yl)phenoxy)benzylidene)-4-nitrobenzohydrazide (7b)

Yield: 88%; **M.pt:** 276–278 °C; **IR (ν_{max} cm^{-1}, KBr):** 3248, 3055, 1654, 1603, 1502, 1345; **^{1}H NMR (400 MHz, δ (ppm) DMSO-d_6):** 12.17 (s, 1H, NH), 8.50 (s, 1H, H_{23}), 8.40 (d, $J = 8.9$ Hz, 2H, H_{29}/H_{31}), 8.18–8.16 (m, 5H, H_{28}/H_{32}, H_{11}/H_{15}, H_5), 8.06 (d, $J = 7.7$ Hz, 1H, H_8), 7.85 (d, $J = 8.8$ Hz, 2H, H_{19}/H_{21}), 7.58–7.54 (m, 1H, H_7), 7.49–7.45 (m, 1H, H_6), 7.28–7.23 (m, 4H, H_{18}/H_{22}, H_{12}/H_{14}); **Anal. Calc. For $C_{27}H_{18}N_4O_4S$:** C, 65.58; H, 3.67; N, 11.33. **Found:** C, 65.51; H, 3.59; N, 11.28.

(E)-N′-(4-(4-(benzo[d]thiazol-2-yl)phenoxy)benzylidene)-4-chlorobenzohydrazide (7c)

Yield: 87%; **M.pt:** 288–290 °C; **IR (ν_{max} cm^{-1}, KBr):** 3245, 3061, 1654, 1484, 1244; **^{1}H NMR (400 MHz, δ (ppm) DMSO-d_6):** 11.91 (s, 1H, NH), 8.48 (s, 1H, H_{23}), 8.17–8.14 (m, 3H, H_{11}/H_{15}, H_5), 8.06 (d, $J = 7.92$ Hz, H_8), 7.96 (d, $J = 8.44$ Hz, 2H, H_{28}/H_{32}), 7.83 (d, $J = 8.52$ Hz, 2H, H_{19}/H_{21}), 7.62 (d, $J = 8.4$ Hz, 2H, H_{29}/H_{31}), 7.58–7.53(m, 1H, H_7), 7.49–7.45 (m, 1H, H_6), 7.26–7.22 (m, 4H, H_{18}/H_{22}, H_{12}/H_{14}); **^{13}C NMR (100 MHz, δ (ppm) DMSO-d_6):** 166.48, 161.99, 158.82, 157.28, 153.58, 147.33, 136.55, 134.41, 132.11, 130.24, 129.51, 129.30, 129.16, 128.55, 128.34, 126.63, 125.39, 122.71, 122.30, 119.47, 119.23; **Anal. Calc. For $C_{27}H_{18}ClN_3O_2S$:** C, 67.01; H, 3.75; N, 8.68. **Found:** C, 66.95; H, 3.70; N, 8.61.

(E)-N′-(4-(4-(benzo[d]thiazol-2-yl)phenoxy) benzylidene)isonicotinohydrazide (7d)

Yield: 80%; **M.pt:** 264–268 °C; **IR (ν_{max} cm^{-1}, KBr):** 3209, 3055, 1645, 1603, 1507, 1411, 1266; **^{1}H NMR (400 MHz, δ (ppm) DMSO-d_6):** 12.10 (s, 1H, NH), 8.81–8.79 (m, 2H, H_{29}/H_{31}), 8.49 (s, 1H, H_{23}), 8.18–8.15 (m, 3H, H_{11}/H_{15}, H_5), 8.06 (d, $J = 7.8$, 1H, H_8), 7.86–7.83 (m, 4H, H_{28}/H_{32}, H_{19}/H_{21}), 7.58–7.54 (m, 1H, H_7), 7.49–7.45 (m, 1H, H_6), 7.28–7.22 (m, 4H, H_{18}/H_{22}, H_{12}/H_{14});**^{13}C NMR (100 MHz, δ (ppm) DMSO-d_6):** 166.47, 161.51, 158.73, 157.47, 153.56, 150.31, 149.67, 148.19, 140.42, 134.39, 129.96, 129.32, 128.37, 126.64, 125.40, 122.71, 122.32, 121.49, 119.44, 119.29; **Anal. Calc. For $C_{26}H_{18}N_4O_2S$:** C, 69.32; H, 4.03; N, 12.44. **Found:** C, 69.26; H, 3.97; N, 12.39.

(E)-N′-(4-(4-(benzo[d]thiazol-2-yl)phenoxy)benzylidene)-4-methoxybenzohydrazide (7e)

Yield: 88%; **M.pt:** 250–254 °C; **IR (ν_{max} cm^{-1}, KBr):** 3247, 3056, 1648, 1605, 1548, 1484, 1285; **^{1}H NMR (400 MHz, δ (ppm) DMSO-d_6):** 11.79 (s, 1H, NH), 8.49 (s, 1H, H_{23}), 8.18–8.14 (m, 3H, H_{11}/H_{15}, H_5), 8.06 (d, $J = 7.88$ Hz, 1H, H_8), 7.94 (d, $J = 8.72$ Hz, 2H, H_{28}/H_{32}), 7.81 (d, $J = 8.4$ Hz, 2H, H_{19}/H_{21}), 7.58–7.54 (m, 1H, H_7), 7.49–7.45 (m, 1H, H_6), 7.21–7.26 (m, 4H, H_{18}/H_{22}, H_{12}/H_{14}), 7.07 (d, $J = 8.8$ Hz, 2H, H_{29}/H_{31}), 3.85 (s, 3H, OCH_3); **^{13}C NMR (400 MHz, δ (ppm) DMSO-d_6):**166.49, 162.46, 158.89, 157.03, 153.56, 146.31, 143.37, 134.39, 130.49, 129.50, 129.29, 129.00, 128.25, 126.63, 125.39, 125.00, 122.69, 122.31, 119.50, 119.16, 113.68, 55.39; **Anal.**

Calc. For $C_{28}H_{21}N_3O_3S$: C, 70.13; H, 4.41; N, 8.76. **Found:** C, 70.09; H, 4.37; N, 8.69.

(E)-N′-(4-(4-(benzo[d]thiazol-2-yl)phenoxy)benzylidene)-4-methylbenzohydrazide (7f)

Yield: 90%; **M.pt:** 246–248 °C; **IR (ν_{max} cm^{-1}, KBr):** 3246, 3055, 1651, 1598, 1502, 1484, 1244; **^{1}H NMR (400 MHz, δ (ppm) DMSO-d_6):** 11.82 (s, 1H, NH), 8.48 (s, 1H, H_{23}), 8.16–8.14 (m, 3H, H_{11}/H_{15}, H_5), 8.06 (d, J = 7.7 Hz, 1H, H_8), 7.83 (dd, J = 12.1, 8.4 Hz, 4H, H_{28}/H_{32}, H_{19}/H_{21}), 7.57–7.53 (m, 1H, H_7), 7.49–7.45 (m, 1H, H_6), 7.35 (d, J = 8.0 Hz, 2H, H_{29}/H_{31}), 7.23 (t, J = 8.6 Hz, 4H, H_{12}/H_{14}, H_{18}/H_{22}), 2.39 (s, 3H, –CH_3); **^{13}C NMR (100 MHz, δ (ppm) DMSO-d_6):** 166.49, 162.86, 158.86, 157.11, 153.56, 146.67, 141.77, 134.39, 130.47, 130.41, 129.29, 129.06, 128.98, 128.27, 127.60, 126.63, 125.39, 122.70, 122.31, 119.49, 119.18, 21.01; **Anal. Calc. For $C_{28}H_{21}N_3O_2S$:** C, 72.55; H, 4.57; N, 9.06. **Found:** C, 72.49; H, 4.51; N, 9.02.

(E)-N′-(4-(4-(benzo[d]thiazol-2-yl)phenoxy)benzylidene)-4-bromobenzohydrazide (7g)

Yield: 89%; **M.pt:** 254–258 °C; **IR (ν_{max} cm^{-1}, KBr):** 3288, 3058, 1651, 1590, 1483, 1549, 1245; **^{1}H NMR (400 MHz, δ (ppm) DMSO-d_6):** 11.95 (s, 1H, NH), 8.47 (s, 1H, H_{23}), 8.17–8.15 (m, 3H, H_{11}/H_{15}, H_5), 8.06 (d, J = 8.00 Hz, 1H, H_8), 7.89 (d, J = 8.6 Hz, 2H, H_{28}/H_{32}), 7.83 (d, J = 8.68 Hz, 2H, H_{19}/H_{21}), 7.77 (d, J = 8.48 Hz, 2H, H_{29}/H_{31}), 7.58–7.54 (m, 1H, H_7), 7.49–7.45 (m, 2H, H_6), 7.27–7.22 (m, 4H, H_{18}/H_{22}, H_{12}/H_{14}); **^{13}C NMR (100 MHz, δ (ppm) DMSO-d_6):** 166.49, 162.08, 157.27, 153.56, 147.31, 134.39, 132.42, 131.50, 130.21, 129.69, 129.31, 129.18, 128.32, 126.65, 125.51, 125.41, 122.70, 122.32, 119.47, 119.24; **Anal. Calc. For $C_{27}H_{18}BrN_3O_2S$:** C, 61.37; H, 3.43; N, 7.95. **Found:** C, 61.31; H, 3.35; N, 7.86.

(E)-N′-(4-(4-(benzo[d]thiazol-2-yl)phenoxy)benzylidene) nicotinohydrazide (7h)

Yield: 80%; **M.pt:** 282–284 °C; **IR (ν_{max} cm^{-1}, KBr):** 3429, 3198, 3052, 1644, 1602, 1507, 1481, 1264; **^{1}H NMR (400 MHz, δ (ppm) DMSO-d_6):** 12.05 (s, 1H, NH), 9.08 (d, J = 1.76 Hz, 1H, H_{32}), 8.78 (dd, J = 4.80, 1.52 Hz, 1H, H_{30}), 8.47 (s, 1H, H_{23}), 8.27 (dt, J = 8.0, 1.8 Hz, 1H, H_{28}), 8.18–8.14 (m, 3H, H_{11}/H_{15}, H_5), 8.06 (d, J = 7.96 Hz, 1H, H_8), 7.84 (d, J = 8.72 Hz, 2H, H_{19}/H_{21}), 7.61–7.54 (m, 2H, H_{29}, H_7), 7.49–7.45 (m, 1H, H_6), 7.27–7.23 (m, 4H, H_{18}/H_{22}, H_{12}/H_{14}); **^{13}C NMR (100 MHz, δ (ppm) DMSO-d_6):** 166.48, 161.61, 158.77, 157.36, 153.56, 152.27, 148.53, 147.59, 135.43, 134.39, 130.08, 129.31, 129.24, 129.13, 128.33, 126.64, 125.40, 123.60, 122.70, 122.32, 119.45, 119.26; **Anal. Calc. For $C_{26}H_{18}N_4O_2S$:** C, 69.32; H, 4.03; N, 12.44. **Found:** C, 69.28; H, 3.97; N, 12.38.

(E)-N′-(4-(4-(benzo[d]thiazol-2-yl)phenoxy)benzylidene) furan-2-carbohydrazide (7i)

Yield: 81%; **M.pt:** 240–246 °C; **IR (ν_{max} cm^{-1}, KBr):** 3229, 3057, 1655, 1590, 1503, 1481, 1289, 1017; **^{1}H NMR (400 MHz, δ (ppm) DMSO-d_6):** 11.88 (s, 1H, NH), 8.48 (s, 1H, H_{23}), 8.17–8.14 (m, 3H, H_{11}/H_{15}, H_5), 8.06 (d, J = 8.0 Hz, 1H, H_8), 7.97 (s, 1H, H_{30}), 7.80 (d, J = 8.76 Hz, 2H, H_{19}/H_{21}), 7.58–7.53 (m, 1H, H_7), 7.49–7.45 (m, 1H, H_6), 7.32–7.31 (d, J = 2.32, 1H, H_{28}), 7.26–7.21 (m, 4H, H_{18}/H_{22}, H_{12}/H_{14}), 6.72 (dd, J = 3.49, 1.74 Hz, 1H, H_{29}); **^{13}C NMR (100 MHz, δ (ppm) DMSO-d_6):** 166.48, 158.84, 157.17, 154.13, 153.56, 147.01, 146.60, 145.81, 134.39, 130.25, 129.29, 129.10, 128.28, 126.63, 125.39, 122.70, 122.31, 119.48, 119.18, 114.88, 112.07; **Anal. Calc. For $C_{25}H_{17}N_3O_3S$:** C, 68.32; H, 3.90; N, 9.56. **Found:** C, 68.27; H, 3.82; N, 9.48.

(E)-N′-(4-(4-(benzo[d]thiazol-2-yl)phenoxy)benzylidene) thiophene-2-carbohydrazide (7j)

Yield: 83%; **M.pt:** 258–260 °C; **IR (ν_{max} cm^{-1}, KBr):** 3260, 3145, 1638, 1597, 1481, 1251; **^{1}H NMR (400 MHz, δ (ppm) DMSO-d_6):** 11.87 (s, 1H, NH), 8.46 (s, 1H, H_{23}), 8.17–8.14 (m, 3H, H_{11}/H_{15}, H_5), 8.07–8.05 (m, 1H, H_8), 7.98–7.82 (m, 4H, H_{19}/H_{21} H_{30}, H_{28}), 7.58–7.54 (m, 1H, H_7), 7.49–7.45 (m, 1H, H_6), 7.27–7.23 (m, 5H, H_{29}, H_{18}/H_{22}, H_{12}/H_{14}); **^{13}C NMR (100 MHz, δ (ppm) DMSO-d_6):** 166.48, 161.21, 158.86, 154.37, 153.56, 146.73, 143.25, 134.74, 134.39, 132.89, 132.30, 130.26, 129.29, 128.27, 127.58, 126.63, 125.39, 122.70, 122.31, 119.68, 119.15; **Anal. Calc. For $C_{25}H_{17}N_3O_2S_2$:** C, 65.91; H, 3.76; N, 9.22. **Found:** C, 65.83; H, 3.70; N, 9.18.

(E)-N′-(4-(4-(benzo[d]thiazol-2-yl)phenoxy)benzylidene)-3-methylbenzohydrazide (7k)

Yield: 85%; **M.pt:** 198–200 °C; **IR (ν_{max} cm^{-1}, KBr):** 3429, 3233, 1653, 1482, 1289, 1244; **^{1}H NMR (400 MHz, δ (ppm) DMSO-d_6):** 11.84 (s, 1H, NH), 8.48 (s, 1H, H_{23}), 8.17–8.15 (m, 3H, H_{11}/H_{15}, H_5), 8.06 (d, J = 7.96 Hz, 1H, H_8), 7.82 (d, J = 8.60 Hz, 2H, H_{19}/H_{21}), 7.75–7.72 (m, 2H, H_{28}, H_{32}), 7.58–7.54 (m, 1H, H_7), 7.49–7.42 (m, 3H, H_6, H_{29}, H_{30}), 7.26–7.22 (m, 4H, H_{18}/H_{22}, H_{12}/H_{14}), 2.41 (s, 3H, –CH_3); **^{13}C NMR (100 MHz, δ (ppm) DMSO-d_6):** 166.50, 161.11, 158.86, 157.16, 153.57, 146.80, 137.79, 134.40, 133.36, 132.32, 133.37, 129.31, 129.09, 128.36, 128.29, 128.07, 126.65, 125.41, 124.71, 122.71, 122.35, 119.50, 119.21, 20.93; **Anal. Calc. For $C_{28}H_{21}N_3O_2S$:** C, 72.55; H, 4.57; N, 9.06. **Found:** C, 72.50; H, 4.52; N, 9.01

(E)-N′-(4-(4-(benzo[d]thiazol-2-yl)-2-methoxyphenoxy) benzylidene)benzohydrazide (7 l)

Yield: 83%; **M.pt:** 240–244 °C; **IR (ν_{max} cm^{-1}, KBr):** 3258, 3058, 1651, 1609, 1505, 1483, 1270; **^{1}H NMR (500 MHz, δ (ppm) DMSO-d_6):** 11.81 (s, 1H, NH), 8.44 (s, 1H, H_{23}), 8.15 (d, J = 8.1 Hz, 1H, H_5), 8.09 (d, J = 8.1 Hz, 1H, H_8), 7.92 (d, J = 7.5 Hz, 2H, H_{28}/H_{32}), 7.87–7.86 (m, 1H, H_{15}), 7.74 (d, J = 8.5 Hz, 2H, H_{19}/H_{21}), 7.70 (dd, J = 8.3, 2.0 Hz, 1H, H_{11}), 7.61–7.52 (m, 4H, H_{29}/H_{31}, H_{30}, H_7), 7.49–7.46 (m, 1H, H_6), 7.26 (d, J = 8.3 Hz, 1H, H_{12}), 7.04 (d, J = 8.5 Hz, 2H, H_{18}/H_{22}), 3.91 (s, 3H, –OCH_3); **^{13}C NMR (125 MHz, δ (ppm) DMSO-d_6):** 167.08, 163.56, 159.10, 153.97, 152.09, 147.74, 146.43, 135.05, 133.91, 132.18, 130.82, 129.51, 129.39, 128.94, 128.04, 127.19,

126.02, 123.30, 122.80, 122.54, 121.34, 117.36, 111.66, 56.44; **Anal. Calc. For $C_{28}H_{21}N_3O_3S$:** C, 70.13; H, 4.41; N, 8.76. **Found:** C, 70.09; H, 4.35; N, 8.72.

(E)-N′-(4-(4-(benzo[d]thiazol-2-yl)-2-methoxyphenoxy) benzylidene)-4-nitrobenzohydrazide (7m)

Yield: 87%; **M.pt:** 188–190 °C; **IR (v_{max} cm^{-1}, KBr):** 3230, 3067, 1654, 1600, 1507, 1482, 1346, 1270; **^{1}H NMR (500 MHz, δ (ppm) DMSO-d_6):**12.09 (s, 1H, NH), 8.46 (s, 1H, H_{23}), 8.37 (d, J = 8.5 Hz, 2H, H_{29}/H_{31}), 8.16–8.14 (m, 3H, H_{28}/H_{32}, H_5), 8.09 (d, J = 8.20 Hz, 1H, H_8), 7.87 (d, J = 2.02 Hz, 1H, H_{15}), 7.76 (d, J = 8.82 Hz, 2H, H_{19}/H_{21}), 7.70 (dd, J = 8.26, 2.05 Hz, 1H, H_{11}), 7.58–7.55 (m, 1H, H_7), 7.49–7.46 (m, 1H, H_6), 7.28 (d, J = 8.21 Hz, 1H, H_{12}), 7.05 (d, J = 8.76 Hz, 2H, H_{18}/H_{22}), 3.91 (s, 3H, –OCH_3); **^{13}C NMR (125 MHz, δ (ppm) DMSO-d_6):** 167.05, 161.87, 159.35, 153.97, 152.11, 149.69, 148.85, 146.31, 139.59, 135.05, 131.13, 130.90, 129.59, 129.19, 127.18, 126.02, 124.10, 123.31, 122.81, 122.63, 121.34, 117.33, 111.67, 56.44; **Anal. Calc. For $C_{28}H_{20}N_4O_5S$:** C, 64.11; H, 3.84; N, 10.68. **Found:** C, 64.11; H, 3.84; N, 10.68.

(E)-N′-(4-(4-(benzo[d]thiazol-2-yl)-2-methoxyphenoxy) benzylidene)-4-chlorobenzohydrazide (7n)

Yield: 85%; **M.pt:** 246–250 °C; **IR (v_{max} cm^{-1}, KBr):** 3285, 3067, 1655, 1596, 1483, 1272; **^{1}H NMR (500 MHz, δ (ppm) DMSO-d_6):** 11.87 (s, 1H, NH), 8.44 (s, 1H, H_{23}), 8.15 (d, J = 8.00 Hz, 1H, H_5), 8.09 (d, J = 8.07 Hz, 1H, H_8), 7.94 (d, J = 8.47 Hz, 2H, H_{28}/H_{32}), 7.87 (d, J = 1.74 Hz, 1H, H_{15}), 7.74 (d, J = 8.65 Hz, 2H, H_{19}/H_{21}), 7.69 (dd, J = 8.25, 1.81 Hz, 1H, H_{11}), 7.61 (d, J = 8.47 Hz, 2H, H_{29}/H_{31}), 7.58–7.54 (m, 1H, H_7), 7.49–7.46 (m, 1H, H_6), 7.26 (d, J = 8.25 Hz, 1H, H_{12}), 7.04 (d, J = 8.62 Hz, 2H, H_{18}/H_{22}), 3.91 (s, 3H, –OCH_3); **^{13}C NMR (125 MHz, δ (ppm) DMSO-d_6):** 167.06, 162.44, 159.18, 153.98, 152.09, 148.04, 146.38, 137.00, 135.05, 132.62, 130.84, 129.99, 129.44, 129.40, 129.03, 127.17, 126.01, 123.31, 122.80, 122.55, 121.33, 117.35, 111.65, 56.43; **Anal. Calc. For $C_{28}H_{20}ClN_3O_3S$:** C, 65.43; H, 3.92; N, 8.18. **Found:** C, 65.37; H, 3.90; N, 8.15.

(E)-N′-(4-(4-(benzo[d]thiazol-2-yl)-2-methoxyphenoxy) benzylidene)isonicotinohydrazide (7o)

Yield: 79%; **M.pt:** 274–278 °C; **IR (v_{max} cm^{-1}, KBr):** 3261, 3048, 1660, 1508, 1487, 1409, 1272; **^{1}H NMR (500 MHz, δ (ppm) DMSO-d_6):** 12.03 (s, 1H, NH), 8.79 (d, J = 6.00 Hz, 2H, H_{29}/H_{31}), 8.45 (s, 1H, H_{23}), 8.17 (d, J = 8.00 Hz, 1H, H_5), 8.10 (d, J = 8.00 Hz, 1H, H_8), 7.88 (d, J = 1.69 Hz, 1H, H_{15}), 7.82 (d, J = 6.00 Hz, 2H, H_{28}/H_{32}), 7.76 (d, J = 8.65 Hz, 2H, H_{19}/H_{21}), 7.71 (dd, J = 8.26, 1.78 Hz, 1H, H_{11}), 7.57 (t, J = 7.64 Hz, 1H, H_7), 7.48 (t, J = 7.60 Hz, 1H, H_6), 7.29 (d, J = 8.26 Hz, 1H, H_{12}), 7.05 (d, J = 8.63 Hz, 2H, H_{18}/H_{22}), 3.92 (s, 3H, –OCH_3); **^{13}C NMR (125 MHz, δ (ppm) DMSO-d_6):** 167.06, 161.97, 159.37, 153.97, 152.12, 150.79, 148.94, 146.30, 140.98, 135.05, 130.91, 129.60, 129.15, 127.20, 126.04, 123.32, 122.83, 122.67, 121.98, 121.35, 117.33, 111.68, 56.46; **Anal. Calc. For $C_{27}H_{20}N_4O_3S$:** C, 67.49; H, 4.20; N, 11.66. **Found:** C, 67.46; H, 4.17; N, 11.64.

(E)-N′-(4-(4-(benzo[d]thiazol-2-yl)-2-methoxyphenoxy) benzylidene)-4-methoxybenzohydrazide (7p)

Yield: 87%; **M.pt:** 284–288 °C; **IR (v_{max} cm^{-1}, KBr):** 3238, 1645, 1605, 1500, 1417, 1270; **^{1}H NMR (500 MHz, δ (ppm) DMSO-d_6):** 11.68 (s, 1H, NH), 8.43 (s, 1H, H_{23}), 8.17 (d, J = 7.93 Hz, 1H, H_5), 8.10 (d, J = 8.06 Hz, 1H, H_8), 7.91 (d, J = 8.76 Hz, 2H, H_{28}/H_{32}), 7.87 (d, J = 1.84 Hz, 1H, H_{15}), 7.75–7.70 (m, 3H, H_{19}/H_{21}, H_{11}), 7.60–7.54 (m, 1H, H_7), 7.51–7.46 (m, 1H, H_6), 7.27 (d, J = 8.25 Hz, 1H, H_{12}), 7.05 (m, 4H, H_{18}/H_{22}, H_{29}/H_{31},), 3.92 (s, 3H, –OCH_3), 3.84 (s, 3H, –OCH_3); **^{13}C NMR (125 MHz, δ (ppm) DMSO-d_6):** 167.07, 162.89, 162.44, 158.97, 153.99, 152.09, 147.06, 146.48, 135.06, 130.80, 129.96, 129.67, 129.26, 127.19, 126.02, 125.95, 123.32, 122.84, 122.52, 121.35, 117.38, 114.18, 111.65, 56.45, 55.89; **Anal. Calc. For$C_{29}H_{23}N_3O_4S$:** C, 68.35; H, 4.55; N, 8.25. **Found:** C, 68.31; H, 4.54; N, 8.21.

(E)-N′-(4-(4-(benzo[d]thiazol-2-yl)-2-methoxyphenoxy) benzylidene)-4-methylbenzohydrazide (7q)

Yield: 89%; **M.pt:** 272–278 °C; **IR (v_{max} cm^{-1}, KBr):** 3266, 2958, 1651, 1611, 1499, 1418, 1270; **^{1}H NMR (500 MHz, δ (ppm) DMSO-d_6):** 11.74 (s, 1H, NH), 8.44 (s, 1H, H_{23}), 8.16 (d, J = 7.94 Hz, 1H, H_5), 8.10 (d, J = 8.07 Hz, 1H, H_8), 7.87 (d, J = 1.65 Hz, 2H, H_{15}), 7.83 (d, J = 7.91 Hz, 2H, H_{28}/H_{32}), 7.73 (d, J = 8.51 Hz, 2H, H_{19}/H_{21}), 7.70 (dd, J = 8.29, 1.75 Hz, 1H, H_{11}), 7.58–7.55 (m, 1H, H_7), 7.50–7.46 (m, 1H, H_6), 7.33 (d, J = 7.90 Hz, 2H, H_{29}/H_{31}), 7.27 (d, J = 8.23 Hz, 1H, H_{12}), 7.04 (d, J = 8.52 Hz, 2H, H_{18}/H_{22}), 3.91 (s, 3H, –OCH_3), 2.38 (s, 3H, –CH_3); **^{13}C NMR (125 MHz, δ (ppm) DMSO-d_6):** 167.07, 163.33, 159.04, 153.98, 152.09, 147.42, 146.44, 142.21, 135.05, 131.03, 130.81, 129.59, 129.46, 129.33, 128.06, 127.19, 126.02, 123.31, 122.82, 122.53, 121.34, 117.36, 111.64, 56.44, 21.50; **Anal. Calc. For $C_{29}H_{23}N_3O_3S$:** C, 70.57; H, 4.70; N, 8.51. **Found:** C, 70.54; H, 4.63; N, 8.48.

(E)-N′-(4-(4-(benzo[d]thiazol-2-yl)-2-methoxyphenoxy) benzylidene)-4-bromobenzohydrazide (7r)

Yield: 83%; **M.pt:** 210–212 °C; **IR (v_{max} cm^{-1}, KBr):** 3209, 3057, 1647, 1608, 1492, 1270; **^{1}H NMR (500 MHz, δ (ppm) DMSO-d_6):** 11.87 (s, 1H, NH), 8.44 (s, 1H, H_{23}), 8.15 (d, J = 7.92 Hz, 1H, H_5), 8.09 (d, J = 8.08 Hz, 1H, H_8), 7.88–7.86 (m, 3H, H_{28}/H_{32}, H_{15}), 7.76–7.68 (m, 5H, H_{19}/H_{21}, H_{29}/H_{31}), 7.69 (dd, J = 8.23, 1.68 Hz, 1H, H_{11}), 7.58–7.54 (m, 1H, H_7), 7.49–7.46 (m, 1H, H_6), 7.26 (d, J = 8.25 Hz, 1H, H_{12}), 7.04 (d, J = 8.61 Hz, 2H, H_{18}/H_{22}), 3.91 (s, 3H, OCH_3); **^{13}C NMR (125 MHz, δ (ppm) DMSO-d_6):** 167.04, 162.52, 159.18, 153.99, 152.09, 148.04, 146.38, 135.06, 132.99, 131.96, 130.85, 130.16, 129.44, 129.41, 127.16, 126.00, 125.94, 123.31, 122.80, 122.55, 121.32, 117.35, 111.64, 56.43; **Anal. Calc. For $C_{28}H_{20}BrN_3O_3S$:** C, 60.22; H, 3.61; N, 7.52. **Found:** C, 60.19; H, 3.59; N, 7.50.

(E)-N′-(4-(4-(benzo[d]thiazol-2-yl)-2-methoxyphenoxy) benzylidene)nicotinehydrazide (7s)

Yield: 81%; **M.pt:** 205–208 °C; **IR (v_{max} cm^{-1}, KBr):** 3248, 1647, 1505, 1482, 1417, 1270; **^{1}H NMR (500 MHz, δ (ppm) DMSO-d_6):** 11.97 (s, 1H, NH), 9.09–9.07 (m, 1H, H_{32}), 8.78–8.75 (m, 1H, H_{30}), 8.43 (s, 1H, H_{23}), 8.27–8.25 (m, 1H, H_{28}), 8.16 (d, J = 7.88 Hz, 1H, H_5), 8.10 (d, J = 7.99 Hz, 1H, H_8), 7.88 (d, J = 1.83 Hz, 1H, H_{15}), 7.76 (d, J = 8.72 Hz, 2H, H_{19}/H_{21}), 7.71 (dd, J = 8.25, 1.92 Hz, 1H, H_{11}), 7.59–7.55 (m, 2H, H_{29}, H_7), 7.50–7.47 (m, 1H, H_6), 7.28 (d, J = 8.25 Hz, 1H, H_{12}), 7.05 (d, J = 8.70 Hz, 2H, H_{18}/H_{22}), 3.92 (s, 3H, –OCH_3); **^{13}C NMR (125 MHz, δ (ppm) DMSO-d_6):** 167.05, 162.04, 159.27, 153.98, 152.71, 152.12, 149.02, 148.32, 146.34, 135.89, 135.06, 130.88, 129.70, 129.51, 129.28, 127.18, 126.02, 124.07, 123.32, 122.83, 122.63, 121.34, 117.34, 111.66, 56.45; **Anal. Calc. For $C_{27}H_{20}N_4O_3S$:** C, 67.49; H, 4.20; N, 11.66. **Found:** C, 67.45; H, 4.17; N, 11.64.

(E)-N′-(4-(4-(benzo[d]thiazol-2-yl)-2-methoxyphenoxy) benzylidene)furan-2-carbohydrazide (7t)

Yield: 78%; **M.pt:** 200–203 °C; **IR (v_{max} cm^{-1}, KBr):** 3233, 1655, 1606, 1506, 1479, 1413, 1272, 1231; **^{1}H NMR (500 MHz, δ (ppm) DMSO-d_6):** 11.80 (s, 1H, NH), 8.44 (s, 1H, H_{23}), 8.16 (d, J = 7.91 Hz, 1H, H_5), 8.09 (d, J = 8.06 Hz, 1H, H_8), 7.95 (s, 1H, H_{30}), 7.87 (d, J = 1.84 Hz, 1H, H_{15}), 7.73–7.69 (m, 3H, H_{19}/H_{21}, H_{11}), 7.56 (t, J = 7.56 Hz, 1H, H_7), 7.48 (t, J = 7.58 Hz, 1H, H_6), 7.30–7.26 (m, 2H, H_{28}, H_{12}), 7.03 (d, J = 8.69 Hz, 2H, H_{18}/H_{22}), 6.70 (dd, J = 3.38, 1.65 Hz, 1H, H_{29}), 3.91 (s, 3H, –OCH_3); **^{13}C NMR (500 MHz, δ (ppm) DMSO-d_6):** 167.05, 159.10, 154.59, 153.98, 152.08, 147.75, 147.15, 146.41, 146.23, 135.06, 130.83, 129.43, 129.37, 127.18, 126.01, 123.31, 122.82, 122.54, 121.33, 117.36, 115.29, 112.54, 111.64, 56.43; **Anal. Calc. For $C_{26}H_{19}N_3O_4S$:** C, 66.51; H, 4.08; N, 8.95. **Found:** C, 66.48; H, 4.03; N, 8.91.

(E)-N′-(4-(4-(benzo[d]thiazol-2-yl)-2-methoxyphenoxy) benzylidene)thiophene-2-carbohydrazide (7u)

Yield: 80%; **M.pt:** 220–222 °C; **IR (v_{max} cm^{-1}, KBr):** 3435, 3054, 1651, 1611, 1515, 1396, 1271; **^{1}H NMR (500 MHz, δ (ppm) DMSO-d_6):** 11.83 (s, 1H, NH), 8.42 (s, 1H, H_{23}), 8.17 (d, J = 7.82 Hz, 1H, H_5), 8.11–8.05 (m, 2H, H_8, H_{28}), 7.94–7.91 (m, 1H, H_{30}), 7.87 (d, J = 1.93 Hz, 1H, H_{15}), 7.81–7.72 (m, 2H, H_{19}/H_{21}), 7.71 (dd, J = 8.26, 1.98 Hz, 1H, H_{11}), 7.59–7.55 (m, 1H, H_7), 7.50–7.47 (m, 1H, H_6), 7.27 (d, J = 8.25 Hz, 1H, H_{12}), 7.24–7.21 (m, 1H, H_{29}), 7.06 (d, J = 6.96 Hz, 2H, H_{18}/H_{22}), 3.92 (s, 3H, –OCH_3); **^{13}C NMR (125 MHz, δ (ppm) DMSO-d_6):** 167.06, 161.67, 159.12, 158.98, 153.98, 152.08, 146.43, 143.86, 135.05, 132.24, 130.83, 129.50, 129.40, 128.56, 127.19, 126.03, 123.32, 122.84, 122.52, 121.34, 117.53, 117.37, 111.63, 56.45; **Anal. Calc. For $C_{26}H_{19}N_3O_3S_2$:** C, 64.31; H, 3.94; N, 8.65. **Found:** C, 64.29; H, 3.90; N, 8.62.

(E)-N′-(4-(4-(benzo[d]thiazol-2-yl)-2-methoxyphenoxy) benzylidene)-3-methylbenzohydrazide (7v)

Yield: 88%; **M.pt:** 188–190 °C; **IR (v_{max} cm^{-1}, KBr):** 3230, 1648, 1609, 1417, 1482, 1271; **^{1}H NMR (500 MHz, δ (ppm) DMSO-d_6):** 11.77 (s, 1H, NH), 8.44 (s, 1H, H_{23}), 8.15 (d, J = 7.93 Hz, 1H, H_5), 8.09 (d, J = 8.10 Hz, 1H, H_8), 7.88–7.86 (m, 1H, H_{15}), 7.74–7.68 (m, 5H, H_{19}/H_{21}, H_{11}, H_{32}, H_{28}), 7.58–7.55 (m, 1H, H_7), 7.49–7.46 (m, 1H, H_6), 8.43–8.40 (m, 2H, H_{29}, H_{30}), 7.26 (d, J = 8.24 Hz, 1H, H_{12}), 7.04 (d, J = 8.54 Hz, 2H, H_{18}/H_{22}), 3.91 (s, 3H, –OCH_3), 2.51 (s, 3H, CH_3); **^{13}C NMR (125 MHz, δ (ppm) DMSO-d_6):** 167.06, 163.58, 159.07, 153.99, 152.09, 147.55, 146.42, 138.25, 135.06, 133.93, 132.74, 130.82, 129.55, 129.36, 128.82, 128.54, 127.17, 126.00, 125.20, 123.31, 122.80, 122.53, 121.33, 117.36, 111.64, 56.43, 21.42; **Anal. Calc. For $C_{29}H_{23}N_3O_3S$:** C, 70.57; H, 4.70; N, 8.51. **Found:** C, 70.54; H, 4.68; N, 8.49.

α-Amylase inhibition studies

The inhibition studies of compounds **7a–7v** for α-amylase were carried out by adopting the assay procedure as described in literature (Keharom et al., 2016). α-Amylase inhibitory activity was carried out by DNSA method on Systronics Spectrophotometer 166 using acarbose as a reference drug.

All the compounds and standard drug were dissolved in dimethyl sulphoxide (DMSO). A stock solution of 1 mg/mL concentration was prepared by using the DMSO solvent. Inhibitory potential of all the synthesized derivatives toward α-amylase was tested at three different concentration, that is, 50 µg/mL, 25 µg/mL and 12.5 µg/mL concentrations, respectively. Acarbose was used as a reference drug and the solutions without test samples were used as a control. The α-amylase (*A. oryzae*) enzyme solution having 50 µg/mL concentration was prepared using 20 mM sodium-potassium buffer (pH 6.9). A total of 1 mL of sample solution **7a–7v** at different concentration (12.5, 25, 50 µg/mL) and 1 mL of enzyme solution were mixed and the solution was incubated at 37 °C for 30 min. A 1 mL of starch solution (prepared by dissolving starch (500 mg) in 25 mL of 0.5 N NaOH and heat the solution for 5 min at 100 °C) was then added to each test tubes and the mixture was further incubated for 15 min at 37 °C. The reaction was stopped by adding 1 mL of 96 mM of DNSA solution to each test tube. After shaking the reaction mixture, the closed test tubes were further heated on the water bath for 15 min at 85 °C. Later on, test tubes were further cooled at room temperature and absorbance was measured at 650 nm. Blanks were prepared without enzymes. A control experiment was conducted in the same manner by replacing the drug sample with 1 mL DMSO. Inhibition percentage of α-amylase was calculated by the following mathematical equation (Nickavar & Yousefian, 2010)

$$\%\ \text{Inhibition} = (\text{Control-Test})/\text{Control} \times 100$$

8.1. QSAR building

8.1.1. Method for QSAR model development

The predictive QSAR model between $pPI_{\alpha\text{–amylase}}$ and correlation weight was built by using Monte Carlo method present in CORAL software. The SMILES and quasi SMILES based descriptor can be calculated by the summation of the

correlation weights (CWs) of diverse SMILES attributes. The balance of correlation approach was used to build QSAR models and the endpoint ($pPI_{\alpha-amylase}$) was calculated by the following mathematical equations (Kumar & Kumar, 2019; Veselinovic et al., 2013)

$$pPI_{\alpha-amylase} = f(SMILES\$) \text{ or } f(SMILES\%) \text{ or } f(SMILES\&) \quad (2)$$

$$pPI_{\alpha-amylase} = C0 + C1 \times^{SMILES\$ \text{ or } SMILES\% \text{ or } SMILES\%} DCW\ (T, N_{epoch}) \quad (3)$$

Here, $, % and & are quasi-SMILES notation for 50, 25 and 12.5 μg/mL concentration.

The optimal descriptor DCW was calculated by the following equation:

$$\begin{aligned} SMILES_{DCW(T,\ N_{epoch})} &= \sum CW(S_K) + \sum CW(SS_K) \\ &+ \sum CW(SSS_K) + CW(BOND) + CW(HALO) \\ &+ CW(NOSP) + CW(PAIR) + CW(C_{max}) + CW(N_{max}) \\ &+ CW(O_{max}) + CW(S_{max}) \end{aligned} \quad (4)$$

Here, $CW(X)$ denotes the correlation weight for the SMILES and quasi-SMILES attributes. T and N_{epoch} denote threshold and number of epoch, respectively. The threshold 'T' is applied to classify the molecular attributes into two classes (i) rare (noise) and (ii) active. A detailed description of global SMILES attributes is outlined in Table 4 (Ahmadi et al., 2020; Toropova & Toropov, 2019a).

Balance of correlation (**TF_1**) and balance of correlation with IIC (**TF_2**) are the two target functions in Monte Carlo Optimization used for QSAR building (Toropova et al., 2015; Veselinovic et al., 2015). In the literature, the role of IIC has been suggested as a novel yardstick to predict the predictive potential of developed QSAR models

$$TF_1 = R_{training} + R_{invTraining} - \left| R_{training} - R_{invTraining} \right| \times Const \quad (5)$$

$$TF_2 = TF_1 + IIC_{SET} \times W_{IIC} \quad (6)$$

The $R_{training}$ and $R_{invTraining}$ are correlation coefficients for the training and invisible training sets, respectively. The empirical constant (Const) and weight of IIC (W_{IIC}) are usually constant (Ahmadi et al., 2019; Toropova et al., 2015; Veselinovic et al., 2015). The following equation is implemented to compute the index of IIC of a particular set (Kumar et al., 2019a; Toropov & Toropova, 2018; Toropova & Toropov, 2017; Toropova & Toropov, 2019a; Toropova et al., 2019)

$$IIC_{SET} = R_{SET} \times \frac{\min(^{-}MAE_{SET}, ^{+}MAE_{SET})}{\max(^{-}MAE_{SET}, ^{+}MAE_{SET})} \quad (7)$$

Here, the R_{SET} is the correlation coefficient value between the observed and predicted endpoint of a typical set. MAE is mean absolute error which can be computed by the following mathematical equation:

$$^{-}MAEset = \frac{1}{^{-}N}\sum_{k=1}^{^{-}N} |\Delta_k| \Delta_k < 0, \ ^{-}N \text{ is the number of } \Delta_k < 0 \quad (8)$$

$$^{+}MAEset = \frac{1}{^{+}N}\sum_{k=1}^{^{+}N} |\Delta_k| \Delta_k \geq 0, \ ^{+}N \text{ is the number of } \Delta_k \geq 0 \quad (9)$$

Here

$$\Delta_k = observed_k - Predicted_k = Y_{obs} - Y_{pred} \quad (10)$$

The values from 1 to 15 for threshold (T) and 1 to 50 for N_{epoch} were used to attain the most predictive arrangement of T and N_{epoch} for all splits. The dR_{weight} and D_{limit} were 0.1. The weight of the index of ideality of correlation (IIC_{weight}) was 0.2. The optimization D_{start} step was 0.1*CW(SA). Here, CW(SA) is the correlation weight of the structural attribute (SA) at the start. The number of probes of optimization was 3.

8.1.2. Validation

The prime goal of the developed QSAR model is to form a robust model that is capable of predicting the properties of a novel molecule in a purposeful, authentic and accurate way.

The robustness and reliability of a developed QSAR model can be decided based on the following methods: (a) cross-validation or internal validation with the training set data; (b) external validation reckon with the test set data and (c) data randomization or Y-scrambling. The Monte Carlo based QSAR models are validated by successfully implementing these methods. The certain statistical parameters such as correlation coefficient (r^2), concordance correlation coefficient (CCC), cross-validated correlation coefficient (q^2), the correlation coefficient for external data (r^2_{ext}), Q^2_{F1}, Q^2_{F2}, Q^2_{F3}, validation metrics, mean absolute error (MAE), Fischer ratio (F) and novel metrics (Rm^2 and MAE based metric) were used to validate the developed QSAR models (Hossain & Roy, 2018; Khan et al., 2019a, 2019b; Kumar et al., 2019c; Ojha & Roy, 2018; Roy, 2015). These parameters were also compared with IIC to review the predictive potential of developed QSAR models (Ahmadi, 2020; Kumar et al., 2019a).

8.1.3. Applicability domain

The parameters or descriptions used in the development of QSAR models must be explanatory. Mechanistic elucidation of established QSAR models assists in the comprehension of the effect of descriptors in the predictive activity. The AD analysis allows us to explore whether the constructed QSAR model can be applied to any set of molecules. In the formulation of the QSAR model, the AD of molecules executes a decisive role in assessing the uncertainty in the prediction of a specific molecule in terms of how alike it is to the molecules used to formulate the model. Therefore, the prediction of a modelled endpoint using QSAR is only significant when the molecule being predicted falls within the AD of the developed QSAR model. Therefore, AD can be expressed as physicochemical, biological or structural space information, based on which a training set of the model is constructed, and the model is applied to make predictions for new molecules within the specific domains (Kumar et al., 2019a). In

the QSAR model built by CORAL Software, AD is calculated by arranging SMILES attributes in the training and calibration sets. If a compound falls outside the range of AD, it is labelled as an outlier. In the CORAL QSAR model, the AD is defined in consonance with the distribution of SMILES characteristics in training and calibration sets as two steps:

Step 1: The definition of statistical defects ($d(F_K)$) for each of the SMILES attributes included to construct the model:

$$d(F_K) = \frac{P_T(A_K) - \mathrm{P_C(A_K)}}{N_T(A_K) + N_C(A_K)} \tag{11}$$

where $P_T(A_K)$ and $P_C(A_K)$ are probabilities of attributes A_K in training and calibration set, respectively; $N_T(A_K)$ and $N_C(A_K)$ are the frequency of attributes A_K in the training set and calibration sets, respectively.

Step 2: the calculation for all substances the statistical SMILES defect (D_j):

$$D_j = \sum_{K=1}^{NA} d(F_K) \tag{12}$$

where NA is the number of non-blocked SMILES attributes in the SMILES.

In the current statistical calculation, a compound falls in AD if

$$D_j < 2 \times \overline{\mathrm{DefectNS}} \tag{13}$$

Here, $\overline{\mathrm{DefectNS}}$ is the average of the statistical SMILES defect for the training set.

8.2. Docking studies

Marvin sketch was used for preparing the optimized 3D structure of compounds **7n**. The protein data bank was assessed for the PDB structure of α-amylase for *A. oryzae* (**PDB ID: 7TAA**) (http://www.rcsb.org/pdb). The protein was prepared by using UCSF Chimera 1.10 (Pettersen et al., 2004) in which co-crystallized ligand and solvent molecules were removed to avoid interference in binding interactions. Missing side-chain gaps were filled using Dun Brack Rotamer Library (Dunbrack, 2002). Gasteiger charges were calculated using AMBERf14SB and antechamber (Wang et al., 2006) and hydrogens were added. The docking studies were performed using Auto Dock Vina 1.1.2 (Trott & Olson, 2010). Grid center with following size center_x = 38.1433640994, center_y = 39.1685534078, center_z = 31.0477751774, size_x = 25.0, size_y = 25.0 and size_z = 25.0 was placed on the active site. The results of docking studies were analysed using Desmond interface.

8.3. MD simulations

The molecular dynamics simulation of the docked complex of 7TAA.pdb with **7n** was performed for 100 ns using Desmond module of Schrödinger 2019-4 to establish the stability of the docked complex (Guo et al., 2010). The docked poses of protein ligand complexes were used as input structures and each complex was prepared by system setup option in Desmond module. Explict solvent system with OPLS2005 force field was used for this simulation study. Orthorhombic periodic boundary condition for 10 Å buffer region was used for solvation of molecular system with crystallographic water (TIP3P) (Jorgensen et al., 1983) and the system was neutralised by adding Na^+ as counter ions. An ensemble (NPT) of Nose–Hoover thermostat (Martyna et al., 1992, 1994) and barostat was applied to maintain the constant temperature (300 K) and pressure (1 bar) of the systems, respectively. A limited memory algorithm (Broyden–Fletcher–Goldfarb–Shanno (LBFGS)) was employed with convergence threshold gradient of 1 kcal/mol/Å for energy minimization. The data were collected for every 100 ps, and the obtained trajectory was analyzed with Desmond interphase.

Acknowledgements

The authors are thankful to Dr. Andrey A. Toropov and Dr. Alla P. Toropova for providing CORAL software. The authors are also thankful to their respective universities for providing the infrastructure. Financial support as senior research fellowship (SRF) to M. Duhan by Haryana State Council of Science and Technology is acknowledged for accomplishing this work.

Author contributions

Authors have done equivalent contributions to this work.

Disclosure statement

The authors reported no potential conflict of interest.

Funding

Meenakshi Duhan thanks Haryana State Council of Science and Technology (HSCST) for the award of the research fellowship.

ORCID

Parvin Kumar http://orcid.org/0000-0002-2635-6465

References

Achary, P. G. R., Toropova, A. P., & Toropov, A. A. (2019). Combinations of graph invariants and attributes of simplified molecular input-line entry system (SMILES) to build up models for sweetness. *Food Research International (Ottawa, Ont.)*, *122*, 40–46. https://doi.org/10.1016/j.foodres.2019.03.067

Ahmadi, S. (2020). Mathematical modeling of cytotoxicity of metal oxide nanoparticles using the index of ideality correlation criteria. *Chemosphere*, *242*, 125192. https://doi.org/10.1016/j.chemosphere.2019.125192

Ahmadi, S., Ghanbari, H., Lotfi, S., & Azimi, N. (2020). Predictive QSAR modeling for the antioxidant activity of natural compounds derivatives based on Monte Carlo method. *Molecular Diversity*. https://doi.org/10.1007/s11030-019-10026-9

Ahmadi, S., Mehrabi, M., Rezaei, S., & Mardafkan, N. (2019). Structure–activity relationship of the radical scavenging activities of some natural antioxidants based on the graph of atomic orbitals. *Journal of Molecular Structure*, *1191*, 165–174. https://doi.org/10.1016/j.molstruc.2019.04.103

Angelova, V., Karabeliov, V., Andreeva-Gateva, P. A., & Tchekalarova, J. (2016). Recent developments of hydrazide/hydrazone derivatives and their analogs as anticonvulsant agents in animal models. *Drug Development Research*, *77*(7), 379–392. https://doi.org/10.1002/ddr.21329

Bhatia, R., Kadyan, K., Duhan, M., Devi, M., Singh, R., Kamboj, R. C., & Kumar, P. (2019). A Serendipitous synthesis: SiO_2–HNO_3 mediated oxidative aromatization and regioselective nitration of 1,3,5-trisubstituted-4,5-dihydro-1*H*-pyrazoles. *ChemistrySelect*, *4*(35), 10417–10424. https://doi.org/10.1002/slct.201902285

Bhutani, R., Pathak, D. P., Kapoor, G., Husain, A., Kant, R., & Iqbal, M. A. (2018). Synthesis, molecular modelling studies and ADME prediction of benzothiazole clubbed oxadiazole-Mannich bases, and evaluation of their anti-diabetic activity through in vivo model. *Bioorganic Chemistry*, *77*, 6–15. https://doi.org/10.1016/j.bioorg.2017.12.037

Brayer, G. D., Luo, Y., & Withers, S. G. (1995). The structure of human pancreatic alpha-amylase at 1.8 A resolution and comparisons with related enzymes . *Protein Science: A Publication of the Protein Society*, *4*(9), 1730–1742. https://doi.org/10.1002/pro.5560040908

Cardoso, L. N. F., Nogueira, T. C. M., Rodrigues, F. A. R., Oliveira, A. C. A., dos Santos Luciano, M. C., Pessoa, C., & de Souza, M. V. N. (2017). N-acylhydrazones containing thiophene nucleus: A new anticancer class. *Medicinal Chemistry Research*, *26*(8), 1605–1608. https://doi.org/10.1007/s00044-017-1832-y

Duhan, M., Singh, R., Devi, M., Sindhu, J., Bhatia, R., Kumar, A., & Kumar, P. (2019). Synthesis, molecular docking and QSAR study of thiazole clubbed pyrazole hybrid as α-amylase inhibitor. *Journal of Biomolecular Structure and Dynamics*. 1–31. https://doi.org/10.1080/07391102.2019.1704885

Dunbrack, R. L. Jr. (2002). Rotamer libraries in the 21st century. *Current Opinion in Structural Biology*, *12*(4), 431–440. https://doi.org/10.1016/S0959-440X(02)00344-5

Ferreira, L. G., Dos Santos, R. N., Oliva, G., & Andricopulo, A. D. (2015). Molecular docking and structure-based drug design strategies. *Molecules (Basel, Switzerland)*, *20*(7), 13384–13421. https://doi.org/10.3390/molecules200713384

Gollapalli, M., Taha, M., Javid, M. T., Almandil, N. B., Rahim, F., Wadood, A., Mosaddik, A., Ibrahim, M., Alqahtani, M. A., & Bamarouf, Y. A. (2019). Synthesis of benzothiazole derivatives as a potent α-glucosidase inhibitor. *Bioorganic Chemistry*, *85*, 33–48. https://doi.org/10.1016/j.bioorg.2018.12.021

Guo, Z., Mohanty, U., Noehre, J., Sawyer, T. K., Sherman, W., & Krilov, G. (2010). Probing the alpha-helical structural stability of stapled p53 peptides: Molecular dynamics simulations and analysis. *Chemical Biology & Drug Design*, *75*(4), 348–359. https://doi.org/10.1111/j.1747-0285.2010.00951 https://doi.org/10.1111/j.1747-0285.2010.00951.x

Hernández-Vázquez, E., Salgado-Barrera, S., Ramírez-Espinosa, J. J., Estrada-Soto, S., & Hernández-Luis, F. (2016). Synthesis and molecular docking of N′-arylidene-5-(4-chlorophenyl)-1-(3,4-dichlorophenyl)-4-methyl-1H-pyrazole-3-carbohydrazides as novel hypoglycemic and antioxidant dual agents . *Bioorganic & Medicinal Chemistry*, *24*(10), 2298–2306. https://doi.org/10.1016/j.bmc.2016.04.007

Hossain, K. A., & Roy, K. (2018). Chemometric modeling of aquatic toxicity of contaminants of emerging concern (CECs) in *Dugesia japonica* and its interspecies correlation with daphnia and fish: QSTR and QSTTR approaches. *Ecotoxicology and Environmental Safety*, *166*, 92–101. https://doi.org/10.1016/j.ecoenv.2018.09.068

Jorgensen, W. L., Chandrasekhar, J., Madura, J. D., Impey, R. W., & Klein, M. L. (1983). Comparison of simple potential functions for simulating liquid water. *The Journal of Chemical Physics*, *79*(2), 926–935. https://doi.org/10.1063/1.445869

Karelson, M., Lobanov, V. S., & Katritzky, A. R. (1996). Quantum-chemical descriptors in QSAR/QSPR Studies. *Chemical Reviews*, *96*(3), 1027–1044. https://doi.org/10.1021/cr950202r

Kaur, I., Khajuria, A., Ohri, P., Kaur, P., & Singh, K. (2018). Benzothiazole based Schiff-base-A mechanistically discrete sensor for HSO_4^- and I^-: Application to bioimaging and vapour phase sensing of ethyl acetate. *Sensors and Actuators B: Chemical*, *268*, 29–38. https://doi.org/10.1016/j.snb.2018.04.072

Keharom, S., Mahachai, R., & Chanthai, S. (2016). The optimization study of α-amylase activity based on central composite design–response surface methodology by dinitrosalicylic acid method. *International Food Research Journal*, *23*(1), 10–17.

Khan, K., Benfenati, E., & Roy, K. (2019a). Consensus QSAR modeling of toxicity of pharmaceuticals to different aquatic organisms: Ranking and prioritization of the DrugBank database compounds. *Ecotoxicology and Environmental Safety*, *168*, 287–297. https://doi.org/10.1016/j.ecoenv.2018.10.060

Khan, P. M., Roy, K., & Benfenati, E. (2019b). Chemometric modeling of *Daphnia magna* toxicity of agrochemicals. *Chemosphere*, *224*, 470–479. https://doi.org/10.1016/j.chemosphere.2019.02.147

Krallinger, M., Rabal, O., Lourenco, A., Oyarzabal, J., & Valencia, A. (2017). Information retrieval and text mining technologies for chemistry. *Chemical Reviews*, *117*(12), 7673–7761. https://doi.org/10.1021/acs.chemrev.6b00851

Kumar, A., & Chauhan, S. (2017). Use of the Monte Carlo method for OECD principles-guided QSAR modeling of SIRT1 inhibitors. *Archiv der Pharmazie (Weinheim)*, *350*(1), e1600268. https://doi.org/10.1002/ardp.201600268

Kumar, P., Bhatia, R., Kumar, D., Kamboj, R. C., Kumar, S., Kamal, R., & Kumar, R. (2015). An economic, simple and convenient synthesis of 2-aryl/heteroaryl/styryl/alkylbenzothiazoles using SiO_2–HNO_3. *Research on Chemical Intermediates*, *41*(7), 4283–4292. https://doi.org/10.1007/s11164-013-1529-x

Kumar, P., Duhan, M., Kadyan, K., Bhardwaj, J. K., Saraf, P., & Mittal, M. (2018). Multicomponent synthesis of some molecular hybrid containing thiazole pyrazole as apoptosis inducer. *Drug Research*, *68*(2), 72–79. https://doi.org/10.1055/s-0043-116947

Kumar, P., Duhan, M., Kadyan, K., Sindhu, J., Kumar, S., & Sharma, H. (2017a). Synthesis of novel inhibitors of α-amylase based on the thiazolidine-4-one skeleton containing a pyrazole moiety and their configurational studies. *MedChemComm*, *8*(7), 1468–1476. https://doi.org/10.1039/c7md00080d

Kumar, P., Kadyan, K., Duhan, M., Sindhu, J., Singh, V., & Saharan, B. S. (2017b). Design, synthesis, conformational and molecular docking study of some novel acyl hydrazone based molecular hybrids as antimalarial and antimicrobial agents. *Chemistry Central Journal*, *11*(1), 115. https://doi.org/10.1186/s13065-017-0344-7

Kumar, P., & Kumar, A. (2019). Nucleobase sequence based building up of reliable QSAR models with the index of ideality correlation using Monte Carlo method. *Journal of Biomolecular Structure and Dynamics*, *38*(11), 3296–3306. https://doi.org/10.1080/07391102.2019.1656109

Kumar, P., & Kumar, A. (2020). CORAL: QSAR models of CB1 cannabinoid receptor inhibitors based on local and global SMILES attributes with the index of ideality of correlation and the correlation contradiction index. *Chemometrics and Intelligent Laboratory Systems*, 200, 103982. https://doi.org/10.1016/j.chemolab.2020.103982

Kumar, P., Kumar, A., & Sindhu, J. (2019a). Design and development of novel focal adhesion kinase (FAK) inhibitors using Monte Carlo method with index of ideality of correlation to validate QSAR. *SAR and QSAR in Environmental Research*, *30*(2), 63–80. https://doi.org/10.1080/1062936X.2018.1564067

Kumar, P., Kumar, A., & Sindhu, J. (2019b). In silico design of diacylglycerol acyltransferase-1 (DGAT1) inhibitors based on SMILES descriptors using Monte-Carlo method. *SAR and QSAR in Environmental Research*, *30*(8), 525–541. https://doi.org/10.1080/1062936X.2019.1629998

Kumar, P., Kumar, A., Sindhu, J., & Lal, S. (2019c). QSAR models for nitrogen containing monophosphonate and bisphosphonate derivatives as human farnesyl pyrophosphate synthase inhibitors based on Monte Carlo method. *Drug Research*, *69*(3), 159–167. https://doi.org/10.1055/a-0652-5290

Kumar, S., Rathore, D. S., Garg, G., Khatri, K., Saxena, R., & Sahu, S. K. (2017c). Synthesis and evaluation of some benzothiazole derivatives as antidiabetic agents. *International Journal of Pharmacy and Pharmaceutical Sciences*, *9*(2), 60–68. https://doi.org/10.22159/ijpps.2017v9i2.14359

Le, T., Epa, V. C., Burden, F. R., & Winkler, D. A. (2012). Quantitative structure–property relationship modeling of diverse materials properties. *Chemical Reviews*, *112*(5), 2889–2919. https://doi.org/10.1021/cr200066h

Macalino, S. J. Y., Gosu, V., Hong, S., & Choi, S. (2015). Role of computer-aided drug design in modern drug discovery. *Archives of Pharmacal Research*, *38*(9), 1686–1701. https://doi.org/10.1007/s12272-015-0640-5

Manisha, Chauhan, S., Kumar, P., & Kumar, A. (2019). Development of prediction model for fructose-1,6-bisphosphatase inhibitors using the Monte Carlo method. *SAR and QSAR in Environmental Research*, *30*(3), 145–159. https://doi.org/10.1080/1062936X.2019.1568299

Martyna, G. J., Klein, M. L., & Tuckerman, M. (1992). Nose–Hoover chains – The canonical ensemble *via* continuous dynamics. *The Journal of Chemical Physics*, *97*(4), 2635–2643. https://doi.org/10.1063/1.463940

Martyna, G. J., Tobias, D. J., & Klein, M. L. (1994). Constant-pressure molecular dynamics algorithms. *The Journal of Chemical Physics*, *101*(5), 4177–4189. https://doi.org/10.1063/1.467468

Mishra, V. R., Ghanavatkar, C. W., Mali, S. N., Qureshi, S. I., Chaudhari, H. K., & Sekar, N. (2019). Design, synthesis, antimicrobial activity and computational studies of novel azo linked substituted benzimidazole, benzoxazole and benzothiazole derivatives. *Computational Biology and Chemistry*, *78*, 330–337. https://doi.org/10.1016/j.compbiolchem.2019.01.003

Murtuja, S., Shaquiquzzaman, M., & Amir, M. (2018). Design, synthesis, and screening of hybrid benzothiazolyl-oxadiazoles as anticonvulsant agents. *Letters in Drug Design & Discovery*, *15*(4), 398–405. https://doi.org/10.2174/1570180814666170526154914

Nickavar, B., & Yousefian, N. (2010). Inhibitory effects of six allium species on α-Amylase enzyme activity. *Iranian Journal of Pharmaceutical Research*, *8*, 53–57.

Nimbhal, M., Bagri, K., Kumar, P., & Kumar, A. (2020). The index of ideality of correlation: A statistical yardstick for better QSAR modeling of glucokinase activators. *Structural Chemistry*, *31*(2), 831–839. https://doi.org/10.1007/s11224-019-01468-w

Ojha, P. K., & Roy, K. (2011). Comparative QSARs for antimalarial endochins: Importance of descriptor-thinning and noise reduction prior to feature selection. *Chemometrics and Intelligent Laboratory Systems*, *109*(2), 146–161. https://doi.org/10.1016/j.chemolab.2011.08.007

Ojha, P. K., & Roy, K. (2018). Development of a robust and validated 2D-QSPR model for sweetness potency of diverse functional organic molecules. *Food and Chemical Toxicology: An International Journal Published for the British Industrial Biological Research Association*, *112*, 551–562. https://doi.org/10.1016/j.fct.2017.03.043

Pettersen, E. F., Goddard, T. D., Huang, C. C., Couch, G. S., Greenblatt, D. M., Meng, E. C., & Ferrin, T. E. (2004). UCSF Chimera – A visualization system for exploratory research and analysis. *Journal of Computational Chemistry*, *25*(13), 1605–1612. https://doi.org/10.1002/jcc.20084

Roy, K. (2015). Application of chemometrics and cheminformatics in antimalarial drug research. *Combinatorial Chemistry & High Throughput Screening*, *18*(2), 89–90. https://doi.org/10.2174/1386207318021502151540l4

Sharma, A. K., Sharma, R., & Gangwal, A. (2018). Surface tension studies of ternary system: Cu(II) surfactants-2-amino-6-methyl benzothiazole complex plus methanol plus benzene at 311 K. *Current Physical Chemistry*, *8*(2), 151–161. https://doi.org/10.2174/1877946808666180914164134

Shi, J., Deng, Q., Li, Y., Zheng, M., Chai, Z., Wan, C., Zheng, Z., Li, L., Huang, F., & Tang, B. (2018). A rapid and ultrasensitive tetraphenylethylene-based probe with aggregation-induced emission for direct detection of α-amylase in human body fluids. *Analytical Chemistry*, *90*(22), 13775–13782. https://doi.org/10.1021/acs.analchem.8b04244

Souza, P. M. D., & Magalhães, P. de O. e. (2010). Application of microbial α-amylase in industry – A review. *Brazilian Journal of Microbiology*, *41*(4), 850–861. https://doi.org/10.1590/S1517-83822010000400004

Svensson, B. (1994). Protein engineering in the alpha-amylase family: Catalytic mechanism, substrate specificity, and stability. *Plant Molecular Biology*, *25*(2), 141–157. https://doi.org/10.1007/BF00023233

Taha, M., Irshad, M., Imran, S., Rahim, F., Selvaraj, M., Almandil, N. B., Mosaddik, A., Chigurupati, S., Nawaz, F., Ismail, N. H., & Ibrahim, M. (2019). Thiazole based carbohydrazide derivatives as α-amylase inhibitor and their molecular docking study. *Heteroatom Chemistry*, *2019*, 1–8. https://doi.org/10.1155/2019/7502347

Taha, M., Ismail, N. H., Lalani, S., Fatmi, M. Q., Atia Tul, W., Siddiqui, S., Khan, K. M., Imran, S., & Choudhary, M. I. (2015). Synthesis of novel inhibitors of α-glucosidase based on the benzothiazole skeleton containing benzohydrazide moiety and their molecular docking studies. *European Journal of Medicinal Chemistry*, *92*, 387–400. https://doi.org/10.1016/j.ejmech.2015.01.009

Taha, M., Shah, S. A. A., Imran, S., Afifi, M., Chigurupati, S., Selvaraj, M., Rahim, F., Ullah, H., Zaman, K., & Vijayabalan, S. (2017). Synthesis and in vitro study of benzofuran hydrazone derivatives as novel alpha-amylase inhibitor. *Bioorganic Chemistry*, *75*, 78–85. https://doi.org/10.1016/j.bioorg.2017.09.002

Thota, S., Rodrigues, D. A., Pinheiro, P. D. S. M., Lima, L. M., Fraga, C. A., & Barreiro, E. J. (2018). N-acylhydrazones as drugs. *Bioorganic & Medicinal Chemistry Letters*, *28*(17), 2797–2806. https://doi.org/10.1016/j.bmcl.2018.07.015

Toropova, A. P., & Toropov, A. A. (2017). The index of ideality of correlation: A criterion of predictability of QSAR models for skin permeability? *The Science of the Total Environment*, *586*, 466–472. https://doi.org/10.1016/j.scitotenv.2017.01.198

Toropova, A. P., & Toropov, A. A. (2019a). QSPR and nano-QSPR: What is the difference? *Journal of Molecular Structure*, *1182*, 141–149. https://doi.org/10.1016/j.molstruc.2019.01.040

Toropova, A. P., & Toropov, A. A. (2019b). Does the index of ideality of correlation detect the better model correctly? *Molecular Informatics*, *38*(8–9), 1800157. https://doi.org/10.1002/minf.201800157

Toropova, A. P., & Toropov, A. A. (2019c). The index of ideality of correlation: Improvement of models for toxicity to algae. *Natural Product Research*, *33*(15), 2200–2207. https://doi.org/10.1080/14786419.2018.1493591

Toropova, A. P., Toropov, A. A., Beeg, M., Gobbi, M., & Salmona, M. (2017). Utilization of the Monte Carlo method to build up QSAR models for hemolysis and cytotoxicity of antimicrobial peptides. *Current Drug Discovery Technologies*, *14*(4), 229–243. https://doi.org/10.2174/1570163814666170525114128

Toropova, A. P., Toropov, A. A., Benfenati, E., Leszczynska, D., & Leszczynski, J. (2015). QSAR model as a random event: A case of rat toxicity. *Bioorganic & Medicinal Chemistry*, *23*(6), 1223–1230. https://doi.org/10.1016/j.bmc.2015.01.055

Toropova, A. P., Toropov, A. A., Veselinovic, A. M., Veselinovic, J. B., Leszczynska, D., & Leszczynski, J. (2019). Semi-correlations combined with the index of ideality of correlation: A tool to build up model of mutagenic potential. *Molecular and Cellular Biochemistry*, *452*(1–2), 133–140. https://doi.org/10.1007/s11010-018-3419-4

Toropov, A. A., & Toropova, A. P. (2018). Predicting cytotoxicity of 2-phenylindole derivatives against breast cancer cells using index of ideality of correlation. *Anticancer Research*, *38*(11), 6189–6194. https://doi.org/10.21873/anticanres.12972

Toropov, A. A., & Toropova, A. P. (2019). Use of the index of ideality of correlation to improve predictive potential for biochemical endpoints. *Toxicology Mechanisms and Methods*, *29*(1), 43–52. https://doi.org/10.1080/15376516.2018.1506851

Toropov, A. A., Toropova, A. P., & Benfenati, E. (2019). The index of ideality of correlation: QSAR model of acute toxicity for Zebrafish (*Danio rerio*) embryo. *International Journal of Environmental Research*, *13*(2), 387–394. https://doi.org/10.1007/s41742-019-00183-y

Trott, O., & Olson, A. J. (2010). AutoDock Vina: Improving the speed and accuracy of docking with a new scoring function, efficient optimization, and multithreading. *Journal of Computational Chemistry*, *31*(2), 455–461. https://doi.org/10.1002/jcc.21334

Version, M., & 6.2.2. (2014). *calculation module developed by ChemAxon*. http://www.chemaxon.com/products/marvin/marvinsketch/

Veselinovic, A. M., Milosavljevic, J. B., Toropov, A. A., & Nikolic, G. M. (2013). SMILES-based QSAR model for arylpiperazines as high-affinity 5-HT(1A) receptor ligands using CORAL . *European Journal of Pharmaceutical Sciences: Official Journal of the European Federation for Pharmaceutical Sciences*, *48*(3), 532–541. https://doi.org/10.1016/j.ejps.2012.12.021

Veselinovic, J. B., Nikolic, G. M., Trutic, N. V., Zivkovic, J. V., & Veselinovic, A. M. (2015). Monte Carlo QSAR models for predicting organophosphate inhibition of acetycholinesterase. *SAR and QSAR in Environmental Research*, *26*(6), 449–460. https://doi.org/10.1080/1062936x.2015.1049665

Wang, J., Wang, W., Kollman, P. A., & Case, D. A. (2006). Automatic atom type and bond type perception in molecular mechanical calculations. *Journal of Molecular Graphics & Modelling*, *25*(2), 247–260. https://doi.org/10.1016/j.jmgm.2005.12.005